Interactive comment on "New strategies for vertical transport in chemistry-transport models: application to the case of the Mount Etna eruption on March 18, 2012 with CHIMERE v2017r4" by Mathieu Lachatre et al.

1 Answer to Anonymous referee #1, received 16 may 2020

We wish to thank the referee for his/her helpful comments. The comments of the referee are in bold, our answers in normal black, the new elements added to the text are in blue.

1.1 Major comments

Firstly, this paper seeks to address two major concerns regarding vertical transport: 1. Vertical transport is poorly represented in most modern chemistry transport modeling efforts, resulting in excessive numerical (and eventually horizontal) diffusion; and 2. The naïve, or brute-force, solution to this increasing the number of levels in the simulation is expensive. This paper has done an excellent job of exploring answers to the first question, but does not provide any insight into the second.

The two "smart" solutions which the authors propose have their own downsides; the Després and Lagoutière (hereafter DL) advection scheme, while antidiffusive, is also only first-order accurate, while the "directly interpolated winds" (hereafter WRFW) approach violates mass conservation. The utility of the paper would be significantly increased if the authors gave a quantitative assessment of the computational overhead associated with each method and compared it to that associated with the naïve approach. Timing alone, in terms of the number of CPU-hours spent on each simulation, would help with this.

Parameters / Resolution	20	50	99
NODIV-VL	943	1177	1376
WRFW-VL	938	1193	1380
NODIV-DL	957	1193	1389
WRFW-DL	936	1187	1302

Table 1: Number of CPU hours for each simulation setup

The number of CPU hours spent on each simulation is provided in Table **??** above. They do not fit any theoretical scaling. The scaling of the computational load relative to the number of vertical levels n is known to be at least

proportional to n (and proportional to n^2 if the CFL in the vertical direction constrains the timestep). Here our observed the scaling is sub-linear which is unexpected.

Here the configuration was 384 CPUs for CHIMERE and 128 CPUs for WRF. The configuration of CHIMERE is extremely light, with only 1 advected species and no chemistry, so that most likely the meteorological simulation, an extremely complex process with several prognostic variables, was using most of the CPU time, with the CHIMERE CPUs likely spending part of the time waiting for the input meteorological fields, at least in the lightest configuration with 20 model levels. It would have been more efficient in terms of computational time to use fewer CPUs for CHIMERE at least in the simulations with 20 levels to balance the load between meteorology and chemistry, but since the point here was to compare the results of the various simulations we preferred to choose an "all other things being equal approach" where the only change in configutaion between a simulation with 20 levels and its 99-levels counterpart is the number of levels.

This underloading of CHIMERE CPUs is very specific to the present configuration since we advect only one species (typically hundreds of species in a CTM simulation). We have observed that in full-fledge CHIMERE simulations with realistic chemistry and using pre-calculated meteorological fields the scaling of computational time according to the number of vertical levels is linear or superlinear.

Due to these limitations, we are unfortunately not able to use our results to provide a more precise information on computational cost.

Similarly, the lack of mass conservation in the WRFW approach causes serious concern. I applaud the authors for their frankness in discussing this limitation. However I believe that a full understanding of the advantages and drawbacks of each approach demands a fuller discussion of this issue than is currently given in Section 3.2.

In Figure 3, it is not clear to the reader why the total domain mass differs so much between each simulation, and it is critically important to the core question of the paper to know why the mass is changing. Specifically, it would help greatly if the authors could quantify on or with Figure 3: 1. How much mass has been (erroneously) lost through the domain upper boundary, based on integrated vertical mass fluxes at the upper boundary;

In Figure 3 (reproduced below), considering the "NODIV" simulations which are mass conservative, SO_2 mass loss is only due to fluxes through the model upper boundary. For this wind strategy, the differences between 20, 50 and 99 vertical levels are explained by the plume proximity to model upper boundary, which can be observed in Figure 7.

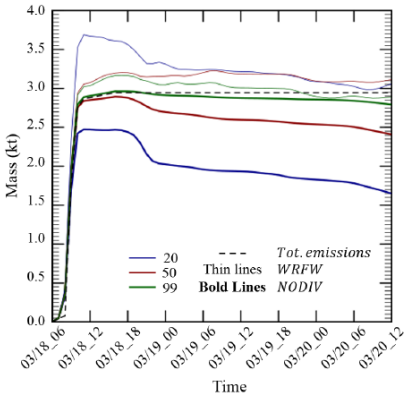

Figure 3. SO_2 mass evolution in model domain (kilotons). Line color indicates the vertical levels configuration, thickness indicates the vertical wind strategy considered. Dotted line represents the cumulated SO_2 mass emitted during Etna volcanic Eruption.

and 2. How much mass has been lost through the domain side boundaries, based on integrated horizontal mass fluxes at the domain boundary. These quantities should enable the authors (and reader) to determine how much of the mass at a given time is spurious, and the degree to which loss through the boundaries is offsetting artificial mass production.

On this note, on lines 2-3 of page 14, the authors mention that the "spurious evolutions in tracer mass become weaker, less than 5 %" once the plume is more diffuse. Does this really mean "the total domain mass is $< 5\,\%$ of the total emitted mass", or is it saying that the amount of mass created spuriously in each time step is $< 5\,\%$ of the current domain total? I assume the former, but if so, does this really mean that the error is $< 5\,\%$, or just that the additional spurious mass is now offset by some loss of mass through the domain boundaries?

The negative trend due to leakage through top of domain is observed mostly in the simulations with 20 and 50 levels. For the simulation with reconstructed wind, this leakage is the only term of mass loss: therefore, we can identify easily the magnitude of this term without additional calculation.

The idea of error compensation is interesting. However, a close look at the curves shows that the decreasing trend due to mass leak at top of model is present in the simulations with interpolated wind as well (thin lines in Fig. 3 reproduced above), and with a comparable magnitude. We think that the effect of mass balance inconsistency due to the divergence of wind field are visible in the small deviations of the curves corresponding to the WRFW simulations around this long-term trend, giving them a more wiggly aspect than those with NODIV which display only a slow and steady decrease. These small movements

$$\frac{\partial \widetilde{C}_{i,j,k}}{\partial t} + \left(\widetilde{F}_{i,j,k+\frac{1}{2}} - \widetilde{F}_{i,j,k-\frac{1}{2}}\right) + \left(\widetilde{F}_{i+\frac{1}{2},j,k} - \widetilde{F}_{i-\frac{1}{2},j,k}\right) + \left(\widetilde{F}_{i,j+\frac{1}{2},k} - \widetilde{F}_{i,j-\frac{1}{2},k}\right) = -\varepsilon_{i,j,k}, \quad (6)$$

are indifferently positive or negative. We think that the effect of this term is not necessarily the effect of "additional spurious mass", but can be indifferently positive and negative as shown by Eq. 6. Actually, errors in discretized calculation of divergence will tend to compensate each other between neighbouring cells, so that we think that the relatively weak effect of the mass inconsistency term as soon as the plume is spread over many cells is due to this error compensation, between neighbouring cells:

If, for example, $\widetilde{F}_{i+\frac{1}{2},j,k}$ is overestimated, this will introduce a negative contribution in $\varepsilon_{i,j,k}$ but a positive and opposite contribution on $\varepsilon_{i+1,j,k}$.

This also explains why the $\varepsilon_{i,j,k}$ term has a much more drastic impact in the first hours of the eruption, because in these hours a substantial part of the total tracer mass is concentrated in one single cell above the vent: then the sign and magnitude of the error term $\varepsilon_{i,j,k}$ in this precise cell becomes critically important and no error compensation occur since the opposite errors on neighbouring cells will act on much smaller tracer concentrations.

Two new paragraphs have been added in Section 3.2 to discuss these points :

In the simulations with the reconstituted non-divergent wind field, substantial mass leak through the top of model can be observed as soon as the injection starts in the 20-level simulation (in which injection is done in the highest model level): the mass of tracer present in the domain never exceeds 85% of the expected mass. For the simulation with 50 vertical levels, this phenomenon is also visible. Another strong episode of mass leak through model top occurs in the simulations with 20 and 50 vertical levels and with reconstructed wind fields from March 18, 18UTC to March 19, 00UTC. This episodes causes an additional drop in tracer mass of 20% in the simulation with 20 levels, 5% in the simulation with 50 vertical levels. This episode of leak also affects the simulation with 20 vertical levels and with interpolated wind fields, reducing tracer mass concentration by about 10% from March 18, 18UTC to March 19, 00UTC. In these three simulations (20 and 50 levels with non-divergent winds, 20 levels with interpolated winds), a continuous decreasing trend in tracer mass is observed throughout the simulation. This drop is directly attributable to leak through model top since the tracer plume is far away from the horizontal boundaries of the domain.

And:

No physical process can explain this overshoot, and it is directly attributable to the choice of lifting the mass conservation constraint in the formulation of transport in order to permit the use of a realistic wind field. If we take March 19, 00UTC as a reference time at which the eruption is terminated, the first strong event of leak through model top is terminated as well, we can observe that the mass evolution in all three WRFW simulations undergoes small variations from

one hour to the next but stay confined in very narrow ranges : 3.3 to 3 kt for the simulation with 20 vertical levels, with a decreasing trend attributable to leakage through model top, 3.1 to 3.25 for the simulation with 50 levels and 2.9 to 3.1 kt for the simulation with 99 vertical levels. The fact that these variations in total mass become marginal in this latter part of plume advection, when the plume is spread over a large geographic areas reflect the fact that numerical errors in the evaluation of divergence mechanically tend to compensate each other between neighbouring cells so that their global impact on a plume that is dispersed over many cells is small.

A broader concern which does not appear to be discussed in detail is the fact that the simulation is driven by fields which are sometimes at a lower vertical resolution. CHIMERE is driven by WRF, running with 33 models, but CHIMERE interpolates this data to its target vertical resolution (Briant et al 2017). Is this interpolation done in a divergence-conserving fashion? If not, does this constitute an uncontrolled-for additional term, in the sense that different vertical grids could introduce different amounts of artificial divergence?

The interpolation of the wind fields is done in a linear fashion which in principle is divergence conserving, but CHIMERE interpolation works directly on winds and not mass fluxes which actually may bring some additional errors in divergence. Our concern was to have all simulations forced with the exact same meteorological simulation, and we decided to retain the typical number of levels that is used in CHIMERE (Briant et al., 2017). The statement that "different vertical grids could introduce different amounts of artificial divergence" is therefore correct. We explicitly draw the reader's attention towards this point in section 2.2.1 of the revised version:

$\varepsilon_{i,j,k}$ depends on the resolution of the meteorological model (which is identical for all our simulations), and on the resolution of the chemistry-transport model, so that this error term that essentially traduces divergence errors due to interpolation depends on the vertical resolution of the model. It is identical between simulations that have the exact same number of domains. Choosing interpolation strategies that reduce this error term is a promising path to mitigating excessive vertical diffusion, as discussed in Emery et al. 2011, but is not investigated here.

Finally, the authors rely heavily on the trajectory of the plume as a metric of the simulation's fidelity. While the equation to determine error (equation 16) is an interesting formulation,

This is true because the plume's horizontal location is the only reliable observation that we had, due to the large uncertainty and error bars in the satellite retrievals of its altitude. Therefore, indicators like the one in Eq. 16 were, unfortunately, our only way to provide a comparison of model simulations with real-world data. We agree that this measure is only an indirect way to observe potential improvements in the vertical direction and reduction in plume diffusion.

(...)it would be helpful to provide a more quantitative assessment of the amount of numerical diffusion. Variation in the maximum

volumetric mixing ratio, (...)

Figure 7 (reproduced below) displays the highest column vertical profile evolution for each simulation. It can be observed that SO_2 mixing ratio is highly impacted by diffusion parameters chosen (please note that the scale use is irregular), and that simulations with the WRFW-DL configurations preserve a much higher maximal VMR than their conterparts with NODIV-VL.

Also, we believe that Figure 8 as well as Figures S5 and S7 in the supplements that have been added in the revised version bring additional elements in this line. Generally speaking, we have chosen to look at a more synthetic parameter like the minimal volume containing 50% of mass plume rather than a value of maximal VMR, which is more dependant on the details of all simulations. Figures 8a and S5 can be directly interpreted in terms of VMR, since the typical VMR in the plume is inversely proportional to plume volume.

(...) the total area of the plume above some minimum VMR, or the total entropy would be useful for quantifying how much numerical diffusion is being introduced.

A calculation very similar to the one suggested by the Referee on area is already present in the manuscript (Section 3.6, Fig 8 of the submitted manuscript and Fig. S5 of the revised manuscript). Here we propose to use the minimum volume containing at least half of the SO_2 mass as a synthetic indicator of how much the plume has been diffused. This is very similar to the proposal of calculating the area above some minimum VMR except that we chose to did it in 3d with volumes instead of areas, and we thought that calculating the volume containing at least half of the plume was a useful method to avoid introducing an arbitry threshold on VMR.

On Figure 8b), we calculate the volume ratios for each parameters (i.e. WRFW vs NODIV; DL vs VL) to provide a quantitative assessment of diffusion reduction on 3 dimensions. To illustrate the differences implied on for plume's surfaces, Figure S6 and Figure S7 (in suppl.) have been added to show the horizontal dispersion of plume on various simulations after 2 days.

We believe that entropy is delicate to interpret for many people including ourselves particularly when, as it is suggested here, we do not speak of a thermodynamic entropy of air but on the artificial construction of a mathematical entropy value for a tracer distribution. We agree that entropy of tracer concentration fields is a useful way of measuring numerical diffusion but we feel that discussing issues in terms of plume volume as we have done is much easier to interpret for the particular case we treat here, as we deal with a physical quantity whose absolute value has a meaning.

This would also allow the authors to account for the effect that spurious vertical diffusion can have in accelerating spurious horizontal diffusion (relevant papers discussing this issue and metrics of numerical diffusion are e.g. Rastigejev et al 2010, Lauritzen and Thuburn 2012, Eastham et al 2017, Zhuang et al 2018).

We agree with the Reviewer that more discussion on this point was useful. The results we obtain are in line with Eastham 2017 and Zhuang 2018: reduction of vertical diffusion has a direct impact on horizontal diffusion as well. Here in

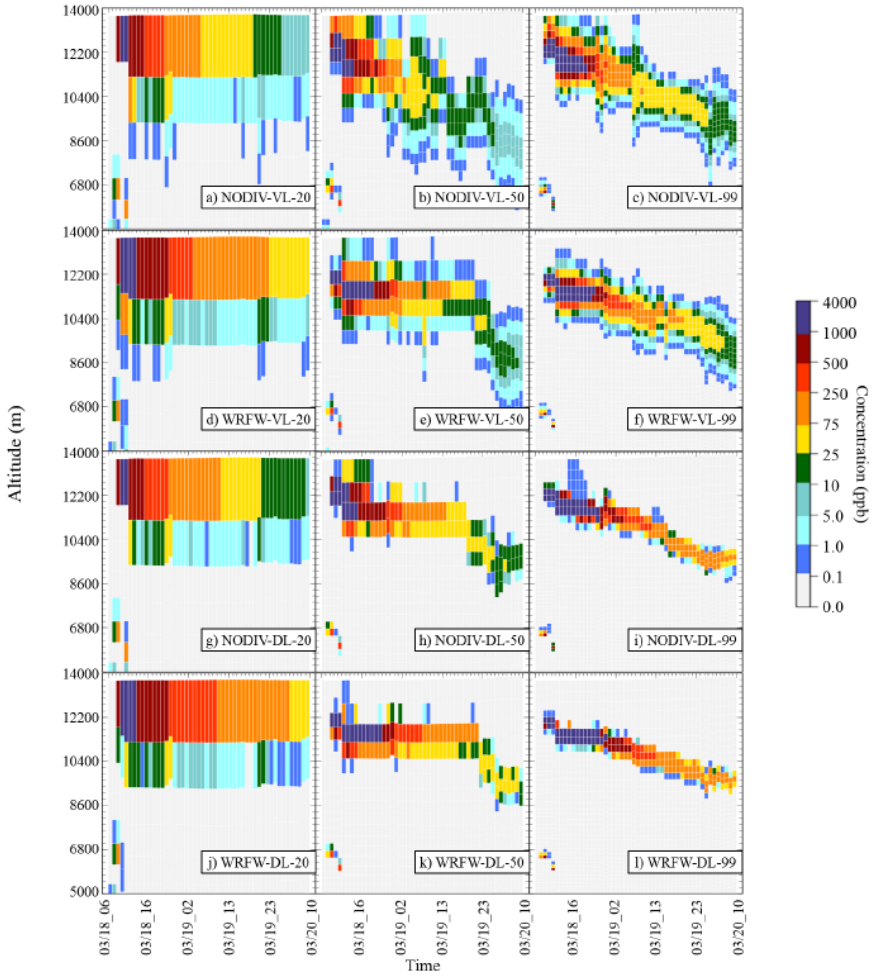

Figure 7. Evolution of SO_2 vertical profile (in ppb) corresponding to the maximum column for each step after the Etna eruption, for each tested model configurations. 1^{st} row: NODIV-VL; 2^{nd} row: NODIV-DL; 3^{rd} row: WRFW-VL; 4^{th} row: WRFW-DL. Left: 20 vertical levels; Center: 50 vertical levels; Right: 99 vertical levels. WRFW simulations values have been corrected to fit NODIV strategy masses.

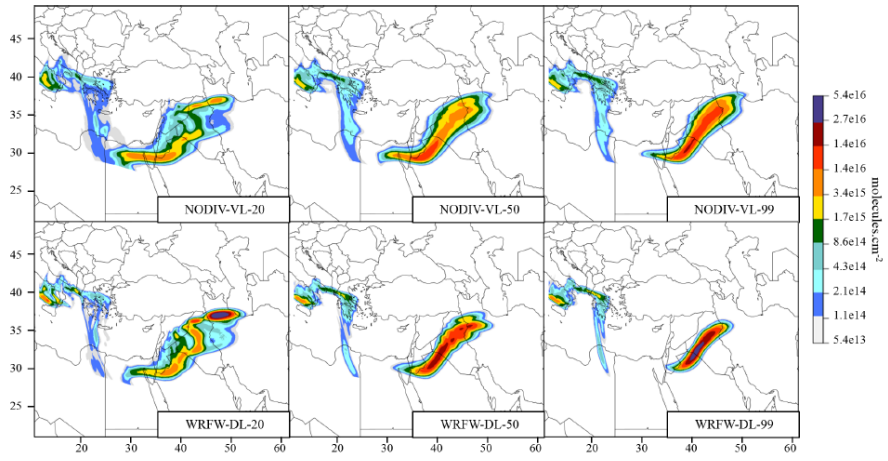

Figure S6. Volcanic plume integrated column dispersion on march 20^{th} at 11 A.M. UTC (2 days after the eruption).

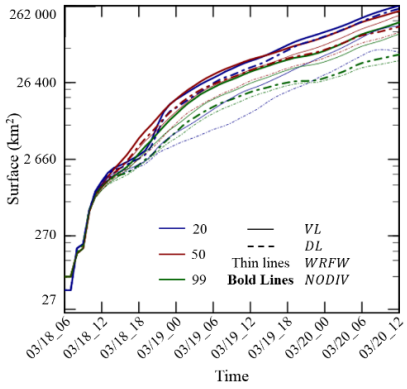

Figure S7. Minimum surface evolution calculated for 50 % of SO_2 total mass in the atmosphere.

the revised version we insist on the finding that this reduction can be obtained not only by improving resolutio but also, to some extent, by the approaches we advocate in the manuscript. A long discussion on this point has been introduced in section 3.6 based on new figures S6 and S7, and a corresponding statement is added in the conclusion as well.

1.2 Minors comments

I believe that there is an error in equation 15. Using the case of a local maximum (i.e. the first term of the Min operator is negative or zero), the estimated cell boundary VMR ends up being the cell mean VMR + 1, when it should presumably by the cell VMR only (specifically if this is meant to recreate the Godunov donor cell scheme for that condition). Although only a technical error, this is critically important to verification of the rest of the paper.

We are deeply grateful to the Referee for this in-depth investigation of our equation. This has permitted us to realize that there was actually a missing multiplicative factor in the equation and that this mistake would have made reproduction of our results in another model very difficult. The correct equation is as follows:

$$\bar{\alpha}_{s,k+\frac{1}{2}} = \alpha_{s,k} + \frac{1-\nu}{2} \mathrm{Max}\left[0, \mathrm{Min}\left(\frac{2}{\nu}\frac{\alpha_{s,k}-\alpha_{s,k-1}}{\alpha_{s,k+1}-\alpha_{s,k}}, \frac{2}{1-\nu}\right)\right] \times \left(\alpha_{s,k+1}-\alpha_{s,k}\right), \tag{1}$$

Even though the last factor was missing, the Referee's interpretation of the behaviour of Eq. 15 is correct and Eq. 15 would result into $\bar{\alpha}_{s,k+\frac{1}{2}} = \alpha_{s,k+1}$ in case of a local maximum, which would in our opinion lead to catastrophic instabilities since mass could never escape from a maximum whose downwind neighbour has zero VMR. As stated in the next sentence of the paper ("if $\left(\left(\alpha_{s,k}-\alpha_{s,k-1}\right)\left(\alpha_{s,k+1}-\alpha_{s,k}\right) \leq 0\right)$, no interpolation is performed and the scheme falls back to the simple Godunov donor-cell formulation"). This sentence may suggest that in case of a maximum the equation naturally falls back to the Godunov donor-cell formula. This is not the case. As we state more clearly in the revised version, Eq. 15 is applied if, and only if, the considered cell is not a local extremum, otherwise $\bar{\alpha}_{s,k+\frac{1}{2}} = \alpha_{s,k}$ is enforced:

As above, Eq. 15 is not applied in the case of a local extremum $\left(\left(\alpha_{s,k}-\alpha_{s,k-1}\right)\left(\alpha_{s,k+1}-\alpha_{s,k}\right) \leq 0\right)$. In this case, $\bar{\alpha}_{s,k+\frac{1}{2}} = \alpha_{s,k}$ is imposed and the scheme falls back to the simple Godunov donor-cell formulation

The same precision is broght for the Van Leer scheme (Eq. 14) since our initial formulation was suffering from the same ambiguity.

Section 2.1: it would be helpful to have details on how the vertical layers are placed (i.e. more detail on the different grid discretizations), and where the cell edges lie relative to the WRF vertical grid.

The various vertical resolutions can be compared on Figure S4 of the revised version.

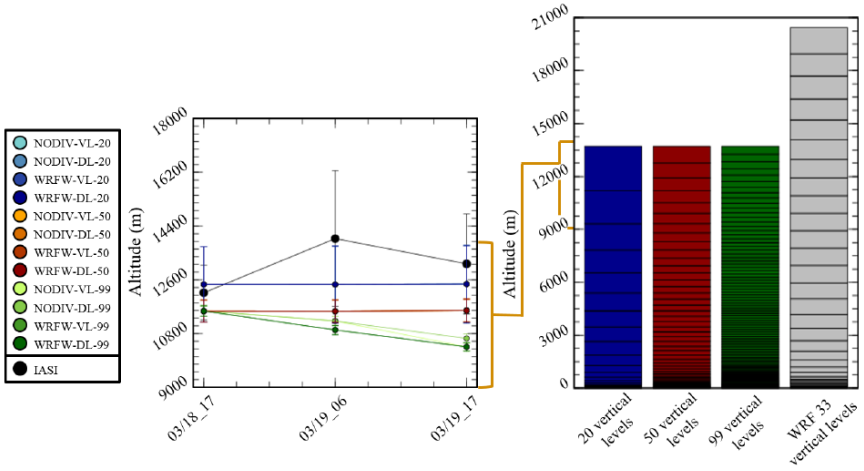

Figure S4. Center : Maximum concentration altitude evolution (IASI and CHIMERE), IASI brackets indicate values' uncertainties and CHIMERE brackets indicates cell's bottom and top. Right : Model vertical levels distribution for the 3 configurations from surface to top.

A sentence has been added to the manuscript :

The WRF model has been run with 33 vertical levels from surface to 55 hPa (28 levels are into 1013-150 hPa range), and with an identical horizontal grid.

P12 L6: 'independant' should be 'independent'

Modification has been done.

P18 L21: Currently this line appears to compare the Després and Lagoutière scheme to itself. Should the second instance actually be "van Leer (1977)"?

Indeed, this has been modified.

P20 L2: Why is increasing vertical resolution only meaningful in cases where plume injection altitude is known? I feel that this statement needs to be better qualified. A reduction in numerical diffusion should always correspond to an improvement in simulation fidelity, even if the initial conditions include error.

We agree with the reviewer that this statement needs to be better qualified. However, we still believe that when increasing accuracy, the probability that the model vertical distribution is totally separated from the real vertical distribution increases. It is true however that, most likely, the qualitative features of the plume including its concentration may be better reproduced in this case even though possible at the wrong location. Therefore, we replaced the question statement by the following which we believe is more precise:

In addition, increasing vertical resolution might give a false appearance of accuracy to the result when plume injection altitude is not known with a good precision.

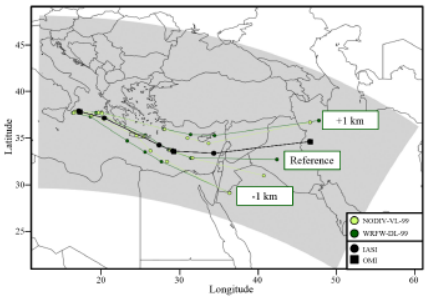

Figure 1. Satellite trajectory of the Etna volcanic plume (black line) built combining information from IASI and OMI instruments. CHIMERE simulated trajectory depending on SO_2 injection altitude of emissions (light and dark green lines - respectively NODIV-VL-99 and WRFW-DL-99). The grey area represents the CHIMERE simulation domain. White triangle indicates Mount Etna location.

1.3 Minor grammatical errors

page 1 line 15, "The CHIMERE CTM has previously been used to assess Eyjajallajökull eruption possible impact on air quality" should be "..to assess the possible impact of the eruption of Eyjajallajökull on air quality").

Phrase formulation has been modified.

I hesitate to bring these up as the errors are almost always very minor and do not impact the science of the paper, and it is usually possible to determine the authors' intended meaning. However, these issues do compromise the readability, and as such I would recommend the authors take another sweep through the paper to correct such issues.

We have performed a thorough checking of grammar and spelling in the manuscript and corrected these slips as best we could.

2 Answer to Anonymous referee #2, received 20^{th} may 2020

We wish to thank the referee for his/her helpful comments. The comments of the referee are in bold, our answers in normal black and the changes that have been brought to the manuscript are in blue.

2.1 General comments

This manuscript presents new numerical modeling approaches to represent vertical transport of pollutants plumes in the upper troposphere with Eulerian Chemistry Transport Models (CTM). The aim is to limit the excessive vertical diffusion of the plumes of pollutant in this kind of numerical representation. Different numerical strategies are considered to address this issue : different vertical wind diagnosis, different advection scheme and different vertical resolution. The sensitivity of the simulation of a plume transport event to the different numerical choices considered in this work is evaluated on the case of the Mount Etna's eruption of March 18, 2012 Its a topic of scientific interest and certainly within the scope of Geoscientific Model Development. The general presentation of the work is logically and clearly organized. However the added value of this work could be improved with the clarification and/or the development of some results.

2.2 Specific Comments

Section 2.1 p4 l7 and l13: Could the authors precise which CHIMERE version has been used? 2013, 2017 or 2016?

Version has been added in the title: *CHIMERE model (v2017r4; Menut et al., 2013; Mailler et al., 2017)*

p4 l14 : The horizontal resolution of the WRF simulation should be mentioned.

This precision has been brought to section 2.1: The horizontal grid is the same as the CHIMERE grid, with a 5 km resolution.

p4 l17 : The authors should provide the limits of the vertical layers (at least in supplement with figure S4).

We agree that some precision was lacking of the model vertical coordinate. However, it would be ewtremely tedious to provide all the vertical levels, and these are not directly human-readable since this a hybrid sigma-pressure coordinate. We have added a brief description of the vertical discretization and refer the reader to the publication where the detail of the discretization strategy is provided:

The discretisation of the vertical levels is as described in [**?**], with vertical levels of exponentially increasing thickness from surface to 850 hPa, and evenly spaced (in pressure coordinates) from 850 hPa. The vertical coordinate depends on the ground-level pressure, with finer vertical levels over elevated ground. The

reader is referred to [**?**] (Section 3.1) for the detailed description of the vertical discretization of the CHIMERE model.

p4 l16-17 : There is an in-depth discussion on the relationship between horizontal resolution and vertical resolution in the article by Zhuang et al. (2018) that the authors cite in the introduction, but nothing is said here on this subject.

A discussion of this aspect is already proposed in the introduction, though not bringing it to the same level as in Zhuang et al. 2018:

p3l8 : *Apart from this wind-mass inconsistency issue, and more specifically for the representation of polluted plumes that are transported over a long range, zhuang et al., (2018) have shown that correct representation of long-range transport of polluted plumes in the free troposphere is severely limited by the insufficient vertical resolution. They show, through dimensional and theoretical arguments, that if* Δx *is not at least several hundred times* Δz*, representation of long-range transport of plumes in the free troposphere is hindered primarily by this coarse vertical resolution, and increasing horizontal resolution does not bring substantial added value in terms of reducing numerical diffusion of the plume. Since the* $\frac{\Delta x}{\Delta z}$ *in typical chemistry-transport models is around or below 20 (with a horizontal resolution of, e.g.,* 20 km *for continental scale studies and vertical resolution of, e.g.,* 1 km*), these authors claim that no major improvement will be reached in the representation of long-range transport plumes unless vertical resolution is refined drastically compared to current typical configurations.*

In the revised version, the reader is explicitly redirected to that study for a more in-depth discussion of this matter:

For a more detailed discussion of the theoretical ground of this relationship between horizontal and vertical discussion, the reader is referred to Zhuang et al., 2018.

Beyond this point, it is weird to see that the chosen vertical extension of the domain does not provide any possibility to reproduce the highest part of the plume as seen by the observations (cf. figure 2e, S3 and S4). All the more so when we see that the meteorological simulation would allow the domain to be extended. Could the authors explain how they chose the different vertical resolutions tested?

The point made by the Referee is a good point. Our choices were to guided by the idea of choosnig typical configurations for chemistry-transport models, including their drawbacks. The Chimere model is not equipped with stratospheric chemistry, and therefore 150hPa is the highest model top value that can be chosen in the model for realistic simulations. Here of course model top could have been extended further up for the need of this particular study since we use inert chemistry, but we have the feeling that leaving the model top at 150hPa permits us to expose more of the problems that occur in typical use of chemistry-transport models, including the discussion of leakage through the model top. This matter is relevant for the simulation of long-range advection in such models, avoiding leakage of the plume through model top, but also for operational air quality forecast since, as has been shown by Emery et

al., (2011), input of stratospheric ozone into the model through spurious mass fluxes at model top significantly affects operational forecast, as discussed in the introduction.

This limitation is explicitly discussed in the revised version:

Section 2.1, The top of model is placed at 150 hPa, with either 20, 50 or 99 vertical layers to evaluate the impact of vertical resolution on the volcanic plume. Even though a higher model top would have been useful for the study of this plume, 150 hPa is a typical value of top of model for CTMs that do not include stratospheric chemistry as it is the case of the CHIMERE model. Also, this relatively low value for top of model permits to examine the question of spurious mass fluxes through the top of model which, as found by Emery et al., (2011) is of relevance not only for long-range transport but also for ozone forecast to ground level.

p4 l17 : These different vertical resolutions rely on an oversampling of the same simulated meteorological fields. Could we expect to get significantly different vertical profile with a meteorological simulation carried out with a finer vertical grid?

Our feeling is that the scale of the vertical wind gradients in the free troposphere (a few thousand meters) is larger than the scale of the change in tracer concentration in a volcanic plume (a few hundred meters because, as discussed in, e.g., Zhang et al 2017, Eastham et al. 2018, these plumes are maintained extremely thin due to the persistant effect of wind sheer). However, we are not able to bring forward a proof of this qualitative argument, and to our knowledge a systematic evaluation of the impact of the vertical resolution of the meteorologic simulation on plume advection in chemistry-transport models is yet to be done.

p4 l17 : Only part of the 33 vertical levels of the meteorological grid is used for the interpolation on the dispersion grid. The number of levels concerned could be specified in this paragraph.

WRF vertical grid has been added to Figure S4 so that the reader can visualize by himself the WRF vertical discretization at the side of the CHIMERE discretization. Also, in Section 2.1, we precise that (28 levels are into 1013-150 hPa range).

p10 l11 and p12 l5: The comparison between the different vertical resolutions involve an aspect which may deserve a bit more detailed discussion. Which kind of boundary conditions are applied for the pollutant concentrations?

We do not have boundary condition for volcanic SO_2. This clarification has been added in the revised version (Section 2.1) :

No boundary conditions were used for SO_2 in our simulations.

We feel that this choice is justified because we are interested in the volcanic plume only. We do not simulate the background SO_2 levels. If we would have made the choice to simulate these background levels, then not only an appropriate boundary condition would have been needed but also a proper set of anthropogenic emissions, which was not the purpose of the present study.

With a plume injection in the last layer of the model (at least when

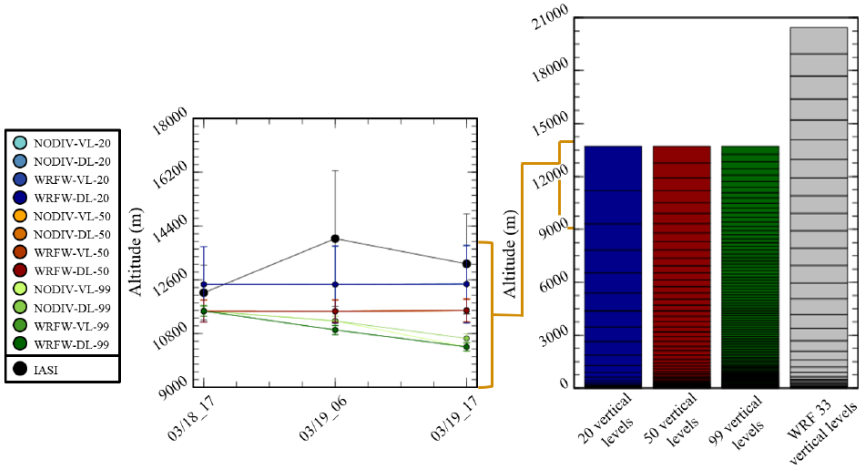

Figure S4. Center : Maximum concentration altitude evolution (IASI and CHIMERE), IASI brackets indicate values' uncertainties and CHIMERE brackets indicates cell's bottom and top. Right : Model vertical levels distribution for the 3 configurations from surface to top.

20 levels are used) it seems that the boundary conditions could play a role. What happens when the flux is downward oriented? (here again the choice of a larger vertical extension would be more relevant).

Because there are no boundary conditions used (or, equivalently, the influx of air into the simulation domain has no SO_2 content), mass that is lost through upper boundary can not be brought back into it if wind turns downward. This is an issue in the 20 vertical levels cases, to a lesser extent to 50 vertical levels cases, compared to 99 vertical resolution cases, where little mass is lost through model upper boundary (q.v. Figure 3).

p13 l1-4 : Could the authors provide the levels concerned in these tests?

The tests have been done one the 3 vertical resolutions. It had no impact on the 20 vertical levels resolution emissions, as eruption profile width was thinner than CHIMERE top level. Only in the 99 vertical level case was observed a slight difference but not really significant on plume trajectory. It has been specified in the document : p13 l14 The tests have been conducted on 20, 50 and 99 vertical levels resolution.

p13 l5-7 : The authors mention an "injection to a unique altitude". It implies the different simulations with the different vertical resolution do not start with the same vertical extension of the plume. It would be interesting to isolate the impact of this initial discrepancy that cannot be associated to an excessive diffusion of the advection scheme. I guess this could be done with a 50 or 99 levels simulations run with an injection uniformly distributed over the different layers corresponding to the injection layer of the 20 levels simulation.

It is possible to see the initial vertical extension of the plume on Figure 7,

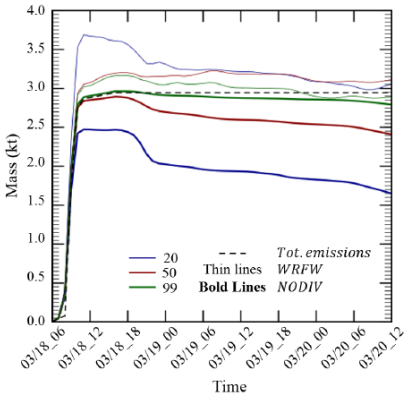

Figure 3. SO_2 mass evolution in model domain (kilotons). Line color indicates the vertical levels configuration, thickness indicates the vertical wind strategy considered. Dotted line represents the cumulated SO_2 mass emitted during Etna volcanic Eruption.

and indeed, simulations do start with different vertical extension of the plume.

We agree that the point brought to our attention by the Reviewer was deserving additional work. We have performed new simulations with a similar injection profile in all simulations, as the reviewer suggests, and we provide the results of these simulations in Figure S5 of the revised manuscript. This new set of simulations permits to have a better quantitative feeling of the results since avoiding the unnatural offset between the different volume curves. We are particularly grateful to the Reviewer for this suggestion.

A paragraph has been added in the manuscript to describe the results :

To evaluate the impact schemes and vertical resolution would have with a similar vertical extension at injection, new simulations have been conducted imposing an identical vertical distribution at the first time (spreading verticaly the emited mass over the same thickness in the 50 and 99-level simulations than it has in the 20-level simulation). Simulations have been conducted for 20, 50 and 99 vertical levels, for WRFW-DL and NODIV-VL parameters, a total of six simulations. Results have been displayed in supplements, on Figure S5. It can be seen on Figure S5 (left) that all plumes have the same initial volume regardless of vertical resolution , which was not the case in the previous case (c.f. Figure 8a). With a larger vertical extension of the plume at injection, volumes are higher than in the "unique cell injection" cases, but resolution and transport scheme influence in the same way the evolution of plume (considering its volume). Figure S5 (right) shows evolutions of SO_2 highest column vertical profile, similar to Figure 7. This new set of experiments show that, even when getting rid of the initial distorsion due to sharper injection profiles in the simulations with the most refined vertical distributions, the increase in plume volume is much slower in the 99-level simulations than in the 20-level simulations. The final volume is about 4 times smaller in the 99-level simulations compared to

their 20-level counterparts. A similar factor in vlume reduction is obtained by changing strategy from VL-NODIV to DL-REALW. In total, final plume volume in the worst-case NODIV-VL-20 simulation is about 20 times bigger than final plume volume in the best-case WRFW-DL-99 simulation.

p14 section 3.3 : With the location of "the model column with the strongest vertically integrated SO2 content" the authors have chosen a very aggregated indicator for the comparison between satellite soundings and model results. I assume this choice was made for sake of simplicity in the presentation of the results. However, seeing that the configuration option can lead to some plume splitting, it would be interesting to have more information concerning the horizontal extension of the plume in the different cases.

The aim of section 3.6 *Parameters impact on SO_2 dispersion* is to evaluate plume diffusion over 3 dimensions (minimum volume containing 50 % of the SO_2 mass), and volume results are applicable to surface (cf. p19 l7: *By extension, it has been observed that volcanic plume shape has been modified by DL and WRFW parameters, reducing the surface area containing 50 % of SO_2 total mass*).

To illustrate the differences, Figure S6 (in suppl.) has been added to show the horizontal dispersion of plume on various simulations after 2 days.

Also, information on the horizontal area of the plume has been added (Fig. S7) and commented briefly in the manuscript: We have also calculated the minimum area containing more than 50% of the SO_2 mass (Fig. S7), showing that the WRFW-DL simulations concentrate 50% of the plume mass in an area at least twice as small as their NODIV-VL counterparts.

p14 l23 : It is not clear to me if the results in figure 5 present average over different configuration options. For instance in the first panel, the simulations with the different advection scheme are compared. Do the number are averages over the different vertical resolutions (the vertical resolution is not mentioned either in the text or in the label of the figure)? Does this imply that there is few interaction between the tested options?

To produce this figure, differences (in km) between model and satellite plumes centroids are calculated for each simulations, then parameters impact are evaluated by calculating the mean between simulation-satellite differences. For instance, "NODIV-DL" (1^{st} line, left column) is the mean between "NODIV-DL-20", "NODIV-DL-50", "NODIV-DL-99". "NODIV-99" (3^{rd} line, left column) is the mean between "NODIV-DL-99" and "NODIV-VL-99". This method has been used to better evaluate the impact of each parameter independently, instead of each simulation. The caption has been expended to help the reader better understand the figure:

To produce this figure, differences (in km) between model and satellite plumes centroids are calculated for each simulation, then parameters impact are evaluated by calculating the mean between simulation-satellite differences. For instance, "NODIV-DL" (1^{st} line, left column) is the mean between "NODIV-DL-20", "NODIV-DL-50", "NODIV-DL-99". "NODIV-99" (3^{rd} line, left column) is the mean between "NODIV-DL-99" and "NODIV-VL-99".

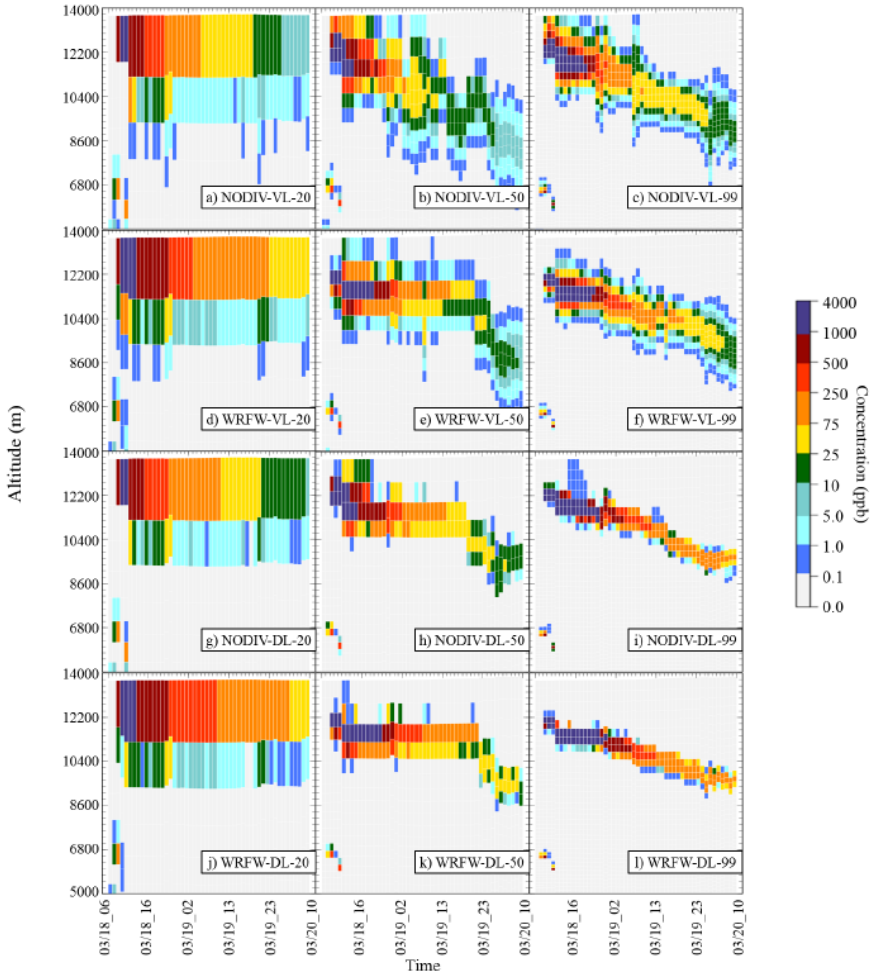

Figure 7. Evolution of SO_2 vertical profile (in ppb) corresponding to the maximum column for each step after the Etna eruption, for each tested model configurations. 1^{st} row: NODIV-VL; 2^{nd} row: NODIV-DL; 3^{rd} row: WRFW-VL; 4^{th} row: WRFW-DL. Left: 20 vertical levels; Center: 50 vertical levels; Right: 99 vertical levels. WRFW simulations values have been corrected to fit NODIV strategy masses.

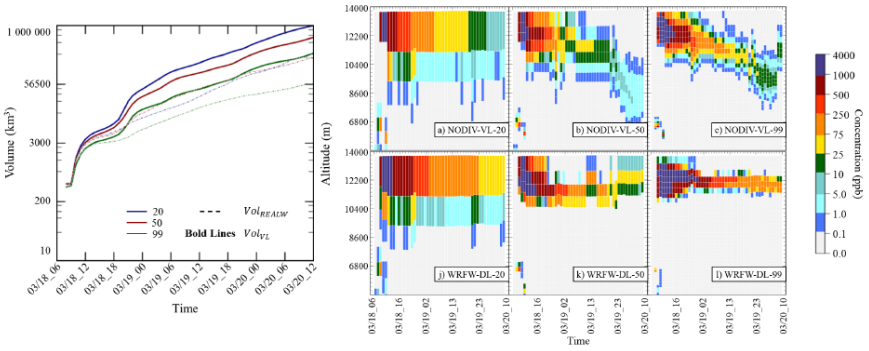

Figure S5. Left) Minimum volume evolution calculated for 50 % of SO_2 total mass in the atmosphere. Right) Evolution of SO_2 vertical profile (in ppb) corresponding to the maximum column for each step after the Etna eruption, for each tested model configurations. 1^{st} row: NODIV-VL; 2^{nd} row: WRFW-DL. Left: 20 vertical levels; Center: 50 vertical levels; Right: 99 vertical levels. WRFW simulations values have been corrected to fit NODIV strategy masses.

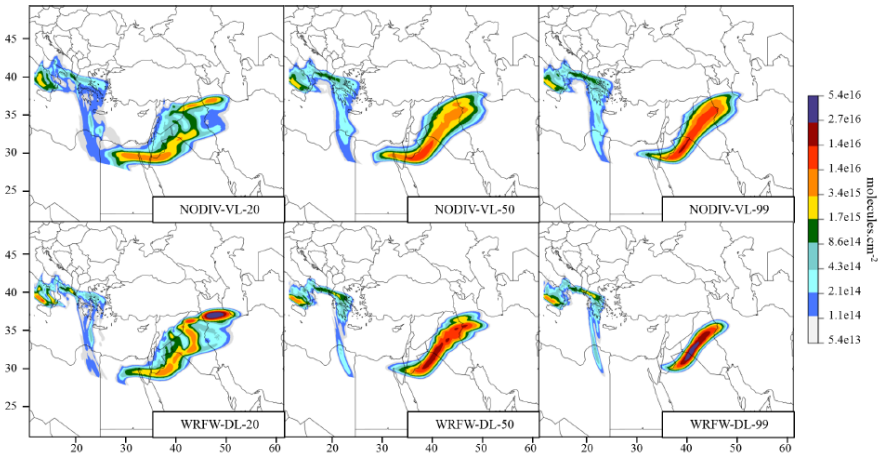

Figure S6. Volcanic plume integrated column dispersion on march 20^{th} at 11 A.M. UTC (2 days after the eruption).

From figure 4 we can see that the WRFW-DL-99 simulation is not the closest to the observation at the final stage. This may not be the intuition get from the results presented.

We present the trajectories to explain what the more synthetic results in, e.g. Fig. 5, mean. It is almost impossible for us to visually extract the information from this set of 12 curves and sort out the effect of all three variable parameters in the simulations, this is why we chose to build more synthetic indices and average simulation ensembles together to isolate as much as possible the effect of the parameters without having too much influence of the good or bad luck that can impact every separate simulation.

On Fig. 4, "WRFW-DL-99" is among a set of, say, 4 simulations that are the closest to the observed satellite plume at final stage, but not the closest.

p16 l18-20 : Could the authors precise how the distribution are built? It is not clear for me if it represents different time steps, different locations, or a mix? Are the observations uncertainties are represented in this figure?

Brackets correspond to distribution's 10^{th} and 90^{th} percentiles (precision now brought to Figures's caption) and observation uncertainties are not represented in this figure: the figure represents only the spread in the satellite-retrieved altitudes and in the modelled altitudes, for the easter plume (above) and the western plume (below), c.f. Figure 2 and Table 3, column 6^{th} ($\lambda_{\mathrm{thr},i}$).

p17 l6-8 : These lines are frustrating from my point of view. The authors focus their work on the excessive vertical diffusion in the dispersion model and the only comparison of the model results to observation concerning the plume vertical extension indicates that this plume property is underestimated. Could the authors provide a more in-depth discussion concerning this point? Some considerations concerning the time evolution of the maximum concentration (modeled and observed) could be useful here to convince the readers that a less diffusive treatment of the advection is really suitable.Since the transport in this application is linear, even a normalized comparison to the "initial" (sounding number 1) maximum concentration would be useful.

We understand the frustration of the Referee about this point, it is our frustration too. However, the large "brackets" in the 10th to 90th percentiles for the satellite measurements are, unfortunately, due only to large uncertainties in the satellite retrievals. In the same line, estimates of maximal concentration in the satellite data are very uncertain, in part but not only due to the uncertainty on the vertical profiles of the satellites. This is why we are able to use comparison to satellite data only to check the general structure of the modelled plume but unfortunately not to give a comparison point on vertical diffusion. Even though we are not able to prove it separately in the present study due to inadequacy of our satellite data for this purpose, we consider that excessive vertical diffusion in Eulerian CTMs are already a well-known and very general problem (e.g. Colette et al. 2010, Emery et al. 2011, Zhuang et al. 2018 etc.).

In the revised version, we add a sentence to explicitly state the limits of the

comparison to satellite data in link with uncertainties of the latter

The dataset also provides error-range estimates along with the retrieved plume altitude. These error-range estimates have a median of around 1000 m in the western plume and 5000 m in the eastern plume, which is much higher aloft. These uncertainties help to understand the wide distribution obtained from satellite. It is also worth noting that this dataset provides pume altitude but does not provide an information on plume thickness. Therefore, comparison between the left and right panels in Figure **??** does not represent the compared plume thickness between model and observation, but the compared variability of plume height. Unfortunately, due to the relatively large ucertainties affecting the retrieved altitudes, no conclusion can be made on this point either. With all these imitations, Fig. **??** prove that model simulations represent the general structure of the pkume, with an elevated eastern plume and a low western plume, and that the median altitudes of both these plumes are very comparable to the median of the satellite-provided altitudes.

2.3 Technical corrections

p5 l11 : It seems an "overbar" is missing for notation consistency. It has been modified, thanks

p11 label table 3 : The last sentence should probably be in the label of Figure 2.

It has been modified.

p18 l21 : erroneous citation

Després and Lagoutière (1999) changed for *Van Leer (1977)*.

New strategies for vertical transport in chemistry-transport models: application to the case of the Mount Etna eruption on March 18, 2012 with CHIMERE v2017r4

Mathieu Lachatre[1], Sylvain Mailler[1,2], Laurent Menut[1], Solène Turquety[1], Pasquale Sellitto[3], Henda Guermazi[3], Giuseppe Salerno[4], Tommaso Caltabiano[4], and Elisa Carboni[5]

[1]LMD/IPSL, École Polytechnique, Institut Polytechnique de Paris, ENS, PSL Université, Sorbonne Université, CNRS, Palaiseau, France.
[2]École des Ponts, Université Paris-Est, 77455 Champs-sur-Marne, France.
[3]Laboratoire Inter-Universitaire des Systèmes Atmosphériques (LISA), UMR CNRS 7583, CNRS, Université Paris Est Créteil et Université de Paris, Institut Pierre Simon Laplace, Créteil, France.
[4]Istituto Nazionale di Geofisica e Vulcanologia, Osservatorio Etneo, Catania, Italy.
[5]Rutherford Appleton Laboratory, Chilton, Didcot, OX11 0QX, Oxfordshire, UK.

Correspondence: Mathieu Lachatre (Mathieu.lachatre@lmd.polytechnique.fr)

Abstract. Excessive numerical diffusion is one of the major limitations in the representation of long-range transport by chemistry-transport models. In the present study, we focus on excessive diffusion in the vertical direction, which has been shown to be a major issue, and we explore three possible ways to address this problem: increase vertical resolution, use an advection scheme with antidiffusive properties, and represent more accurately the vertical wind. This study is done with the CHIMERE chemistry-transport model, for the March 18, 2012 eruption of Mount Etna, which has released about 3 kt of sulphur dioxide in the atmosphere into a plume that has been observed by satellite instruments (IASI and OMI) for several days. The change from the classical Van Leer (1977) scheme to the Després and Lagoutière (1999) antidiffusive scheme in the vertical direction has been shown to bring the largest improvement to model outputs in terms of preserving the thin plume emitted by the volcano. To a lesser extent, improved representation of the vertical wind field has also been shown to reduce plume dispersion. Both these changes help reducing vertical diffusion in the model as much as a brute-force approach (increasing vertical resolution).

1 Introduction

Among many other uses such as operational forecast of air quality, chemistry-transport models (CTM) have been used successfully in the past to represent long-range transport of polluted plumes from different types of sources (mineral dust, volcanic eruptions, biomass burning etc.). The CHIMERE [1] CTM (Mailler et al., 2017) has previously been used to assess the possible impact of Eyjafjallajökull's 2010 eruption ~~possible impact~~ on air quality (Colette et al., 2011). Ash transport from this eruption has been modelled and compared to LiDAR vertical profiles, showing that the CHIMERE model ~~represented~~ represents

[1]www.lmd.polytechnique.fr/chimere/, last consulted 08/28/19

correctly the advection of this volcanic plume from its source in Iceland to the LiDAR (Light Detection And Ranging) facility located in Palaiseau (France), thousands of kilometers away. The altitude, location and timing of the plume was represented correctly, but the authors have shown that their simulation presented a strongly overestimated vertical spread of the plume. Similar studies focusing on volcanic plume dispersion from Boichu et al. (2013) have highlighted overestimations of plume diffusion on 2010 Eyjafjallajökull. Several parameters can influence the evolution of the modelled plume: the emission fluxes and time profile; the injection height and vertical profile; chemical processes involving the considered species; ~~the~~ wind field; ~~the~~ numerical advection schemes and ~~the~~ vertical resolution. Boichu et al. (2015) have focused on volcanic plume dispersion sensitivity to ~~altitude of injection~~ injection altitude, combining CHIMERE and Atmospheric Sounding Interferometer instrument (IASI) for a Mount Etna - study case of an eruption of moderate intensity in April 2011. The eruption presented an emission profile centered at 7 000 m.a.s.l., with weaker emissions at 4 000 m.a.s.l.. These authors found a strong sensitivity of model outputs to the altitude of injection. In Mailler et al. (2017), advection of the volcanic SO_2 plume emitted by a major eruption of the Puyehue Cordó Caulle volcano (Chile) is simulated with the CHIMERE model and compared to satellite measurements and to analyses provided by Klüser et al. (2013). This work shows that, after about one week of simulation, circumpolar transport of the plume has been represented correctly and the final position of the leading edge of the plume is simulated in a reasonable way, but ~~that~~ plume dilution is excessive compared to the observed shape and concentration of the plume.

Most CTMs have been built as offline models forced by meteorological fields, in particular wind and air density, taken from a forcing meteorological model, typically global forecast data such as outputs from the IFS (Integrated Forecasting System) or GFS (Global Forecast System), data from operational forecast centers or data generated by the modellers themselves from a locally run meteorological model. These meteorological data, after interpolation in time and space onto the CTM grid, are used to drive advection within the CTM. However, grid type, grid structure, transport schemes and time discretization are generally different in the CTM from their formulations in the forcing models, deriving into mass-wind inconsistencies: once interpolated onto the CTM grid, the mass and wind fields do not obey the continuity equation anymore (Jöckel et al., 2001). While theoretical pathways to mitigation of this problem exist (Jöckel et al., 2001), this problem has historically been solved practically in regional CTMs in a straightforward way as described in Emery et al. (2011): reconstructing the vertical wind from the density field and the horizontal mass flux divergence in order to artificially enforce verification of the continuity equation to the expense of the realism of the vertical mass fluxes, in particular in the free troposphere. This approach is justified by the fact that, in the lowest atmospheric layers, the reconstructed vertical mass flux is not very different from the real mass flux from the forcing model, and that this explicitly resolved vertical transport is usually dominated by mixing inside the Planetary Boundary Layer (PBL). Therefore, it has long been thought that this approach generates little if any problem since the main purpose of regional CTMs is to provide a reliable forecast of the concentration of pollutants within the PBL. This historic focus on the PBL has also led to the habit of chemistry-transport modellers to use very loose vertical resolution in the free troposphere. Emery et al. (2011) describes the side effects on such an approach in two of the most used CTMs (CAMx and CMAQ). They show that oversimplification of ~~transport processes~~ vertical transport in the free troposphere can not only be detrimental to the representation of transport in the free troposphere itself but also defeats its own purpose: focus on obtaining

a correct representation of pollutant concentrations in the PBL. They have shown that oversimplified representation of vertical transport and vertical mass fluxes in the free troposphere spuriously increases vertical transport of stratospheric ozone into the troposphere, resulting into degraded scores for forecast and analysis of ozone concentration in the PBL, particularly over complex and elevated terrain (springtime in the United States, in the case of Emery et al., 2011). To solve this problem, the authors tried different approaches. While trying to reduce spurious vertical velocities by applying mass filters, smoothers/desmoother filters or divergence minimizers to the forcing velocity field either brings little improvement to the issue or introduces numerical artefacts, improvement of the vertical transport scheme and increase in the vertical number of layers in the free troposphere did bring substantial improvement to the issue of excessive transport of stratospheric ozone into the stratosphere.

Apart from this wind-mass inconsistency issue, and more specifically for the representation of polluted plumes that are transported over a long range, Zhuang et al. (2018) have shown that correct representation of long-range transport of polluted plumes in the free troposphere is severely limited by the insufficient vertical resolution. They show, through dimensional and theoretical arguments, that if Δx is not at least several hundred times Δz, representation of long-range transport of plumes in the free troposphere is hindered primarily by this coarse vertical resolution~~, and increasing horizontal resolution~~. Increasing horizontal resolution in these conditions does not bring substantial added value in terms of reducing numerical diffusion of the plume. Since the $\frac{\Delta x}{\Delta z}$ in typical chemistry-transport models is around or below 20 (with a horizontal resolution of, e.g., $20\,\mathrm{km}$ for continental scale studies and vertical resolution of, e.g., $1\,\mathrm{km}$), these authors claim that no major improvement will be reached in the representation of long-range transport plumes unless vertical resolution is refined drastically compared to current typical configurations. However, they do not examine the use of anti-dissipative transport schemes, which can be a possibility to reduce vertical diffusion without dramatically increasing vertical resolution. For a more detailed discussion of the theoretical ground of this relationship between horizontal and vertical discussion, the reader is referred to Zhuang et al. (2018).

In the present study, three options have been tested in terms of the accuracy of representation of the long-range advection of thin layers. One option is to choose the Després and Lagoutière (1999) anti-diffusive advection scheme for vertical transport, the second option is to use realistic vertical mass fluxes instead of reconstructed vertical mass fluxes, the third option being refinement of vertical resolution. We have chosen the March 18, 2012 Etna volcano eruption to evaluate the impact of these new strategies for vertical transport. This volcano is well monitored, thus allowing to gather detailed model inputs and correlative data. This eruption has been relatively strong, so that the resulting volcanic plume has been distinctly observed and followed by satellite instruments, permitting comparison of modelled to observed plume at different stages of plume evolution over more that two days. Etna volcanic activity is monitored continuously to estimate SO_2 fluxes and plume injection height (Salerno et al., 2009; Mastin et al., 2009; Sellitto et al., 2016; Salerno et al., 2018). Volcanic ~~gas and aerosol~~ gases and aerosols are also subject to numerous physical and chemical evolution processes, such as ~~sulphates~~ sulphate production or CCN activation, ~~whose~~ which have been recently studied (Sellitto et al., 2017; Guermazi et al., 2019; Pianezze et al., 2019) but are not accounted for in this study.

The manuscript is structured in the following way: Material and method (section 2) presents the CHIMERE model configuration for these simulations, including a detailed presentation of the transport formulation and its discretization in the

CHIMERE model, adaptation of the Després and Lagoutière (1999) scheme to the CHIMERE framework and presentation of the method for compensation of mass-wind inconsistencies that permits us to use realistic vertical mass fluxes instead of reconstructed mass fluxes. Also in this section, we discuss the satellite data that we used as a comparison point for our model outputs, the different settings of the performed sensitivity tests and the SO_2 emission fluxes that we use. In the results and discussion (section 3), eruption injection altitude impact on plume transport is first investigated and compared to the plume transport constructed from satellite based instruments. In addition, sensitivity to vertical profile of injection has been evaluated. Then, the dispersion and trajectory of the simulated plumes is discussed and compared to the available data, with a focus on the impact of the various tested parameters on plume dispersion (vertical wind representation, vertical advection scheme and number of vertical levels).

2 Material and methods

2.1 CHIMERE simulations

Simulations have been performed using a development version of the CHIMERE model ~~(Menut et al., 2013; Mailler et al., 2017)~~ (v2017r4; Menut et al., 2013; Mailler et al., 2017) including the new developments presented in section 2.2. The simulations have been performed with no chemistry, and an inert gaseous tracer with the molar mass of SO_2 has been emitted at the location of the Etna volcano, with fluxes and injection heights that are presented below. ~~In particular, oxidation~~ No boundary conditions were used for SO_2 in our simulations. Oxidation of SO_2 and subsequent formation of sulphate or sulfuric acid have not been represented. Simulations last 120 hours starting on March 18, 00 UTC. The CHIMERE model has been forced using WRFv.3.7.1 (Weather Research and Forecasting Skamarock et al., 2008), with an update of the forcing meteorological variables every 20 minutes using the WRF-CHIMERE online simulation framework (Briant et al., 2017). The WRF model has been run with 33 vertical levels from surface to ~~55~~ 55 hPa ~~. Boundary conditions meteorological fields and spectral nudging of the WRF simulation~~ (28 levels are into 1013-150 hPa range). The horizontal grid is the same as the CHIMERE grid, with a 5 km resolution. The meteorological boundary conditions have been taken from the NCEP GFS dataset at 0.25° resolution (NCEP, 2015), also used for the spectral nudging of the WRF simulation. The CHIMERE simulation domain ~~contains~~ is identical to the WRF simulation domain, with 799×399 cells at 5 km resolution. The geometry of the domain, which has a Lambert-conformal projection, is shown in ~~Fig.~~Figure 1. The top of model is placed at 150 hPa, with either 20, 50 or 99 vertical layers to evaluate the impact of vertical resolution on the volcanic plume. Even though a higher model top would have been useful for the study of this plume, 150 hPa is a typical value of top of model for CTMs that do not include stratospheric chemistry as it is the case of the CHIMERE model. Also, this relatively low value for top of model permits to examine the question of spurious mass fluxes through the top of model which, as found by Emery et al. (2011) is of relevance not only for long-range transport but also for ozone forecast to ground level.

The discretisation of the vertical levels is as described in Mailler et al. (2017), with vertical levels of exponentially increasing thickness from surface to 850 hPa, and evenly spaced (in pressure coordinates) from 850 hPa. The vertical coordinate depends

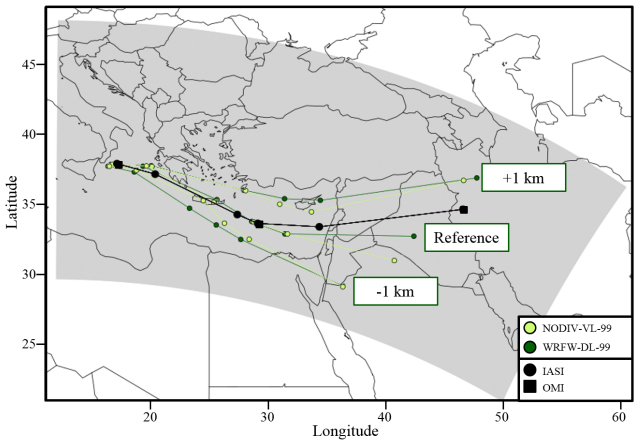

Figure 1. Satellite trajectory of the Etna volcanic plume (black line) built combining information from IASI and OMI instruments. CHIMERE simulated trajectory depending on SO_2 injection altitude of emissions (light and dark green lines - respectively NODIV-VL-99 and WRFW-DL-99). The grey area represents the CHIMERE simulation domain. White triangle indicates Mount Etna location.

on the ground-level pressure, with finer vertical levels over elevated ground. The reader is referred to Mailler et al. (2017) (Section 3.1) for the detailed description of the vertical discretization of the CHIMERE model.

Horizontal advection in the CHIMERE model has been represented using the classical Van Leer (1977) second-order slope-limited transport scheme.

2.2 Discretization of transport

Total concentration for all species together will be noted C (number of gas particles per unit volume; $\mathrm{molec.m^{-3}}$; corresponding to air density), concentration of a particular species s will be noted C_s (number of molecules of species s per unit volume; $\mathrm{molec..m^{-3}}$), mixing ratio for species s will be noted $\alpha_s = \frac{C_s}{C}$. Continuity equation for the motion of air is as follows:

$$\frac{\partial C}{\partial t} + \nabla(\mathbf{\Phi}) = 0, \tag{1}$$

where $\mathbf{\Phi} = C\mathbf{u}$ is the total flux of molecule number.

In the following equations, i, j, k are the indices for the two horizontal directions and the vertical direction respectively, $F_{k+\frac{1}{2}}$ is the mass flux through the top of layer k, positively oriented for upward fluxes. Similarly the horizontal mass fluxes through lateral cell boundaries, positively oriented towards increasing i and j values respectively, are noted $F_{i+\frac{1}{2},j,k}$ and $F_{i,j,k}$. The mass flux components need to verify the discretized form of Eq. 1:

$$\frac{\partial C_{i,j,k}}{\partial t} + \left(F_{i,j,k+\frac{1}{2}} - F_{i,j,k-\frac{1}{2}}\right) + \left(F_{i+\frac{1}{2},j,k} - F_{i-\frac{1}{2},j,k}\right) + \left(F_{i,j+\frac{1}{2},k} - F_{i,j-\frac{1}{2},k}\right) = 0 \tag{2}$$

The continuity equation for species s is as follows:

$$\frac{\partial C_s}{\partial t} + \nabla\left(\mathbf{\Phi}_s\right) = 0 \tag{3}$$

or equivalently:

$$\frac{\partial C_s}{\partial t} + \nabla\left(\alpha_s \mathbf{\Phi}\right) = 0 \tag{4}$$

In CHIMERE, Eq. 4 is discretized as:

$$\begin{aligned}\frac{\partial C_{s,i,j,k}}{\partial t} &+ \left(\bar{\alpha}_{i,j,k+\frac{1}{2}} F_{i,j,k+\frac{1}{2}} - \bar{\alpha}_{i,j,k-\frac{1}{2}} F_{i,j,k-\frac{1}{2}}\right) \\ &+ \left(\bar{\alpha}_{i+\frac{1}{2},j,k} F_{i+\frac{1}{2},j,k} - \bar{\alpha}_{i-\frac{1}{2},j,k} F_{i-\frac{1}{2},j,k}\right) \\ &+ \left(\bar{\alpha}_{i,j+\frac{1}{2},k} F_{i,j+\frac{1}{2},k} - \bar{\alpha}_{i,j-\frac{1}{2},k} F_{i,j-\frac{1}{2},k}\right) = 0\end{aligned} \tag{5}$$

where $\bar{\alpha}$ are the reconstituted values of mixing ratio α on the facet indicated by the indices ($\alpha_{i,j,k+\frac{1}{2}}$ $\bar{\alpha}_{i,j,k+\frac{1}{2}}$ for the top facet of cell i,j,k etc.). If the mass flux values F are such that Eq. 2 is exactly verified, then Eq. 5 ensures that the mixing ratios α_s are not affected by wind-mass discrepancies: in particular, a species with an initially uniform mixing ratio will maintain it after transport is applied. This is why it is so critical for chemistry-transport models to have Eq. 2 verified exactly.

Eq. 5 raise two important questions:

1. How to express the interpolated mixing ratios $\bar{\alpha}_s$, which is the task of the transport scheme ?
2. How to enforce exact verification of Eq. 2 to ensure the absence of mass-wind inconsistencies ?

2.2.1 Vertical wind strategy

In CHIMERE, as in most other chemistry-transport models (Emery et al., 2011), with the notable exception of chemistry-transport modules that are embedded within a meteorological model and use the same grid and time step as it is most notably the case of WRF-CHEM (Grell et al., 2005), the model does not have access to mass flux components $F_{i\pm\frac{1}{2},j\pm\frac{1}{2},k\pm\frac{1}{2}}$ and a density field C that verify Eq. 2. This is a big problem when it comes to advecting species mixing ratios since as we have seen above, the fact that the CTM is able to transport species with Eq. 5 while maintaining uniformity of initially uniform mixing ratios critically depends on that property. Usually, chemistry-transport models rely on the typical outputs of meteorological models, namely the instantaneous values of winds at the meteorological model cell boundaries, and instantaneous values of density. From these variables, it is possible to evaluate the mass fluxes through the CTM cell boundaries, obtaining interpolated mass flux values that are close to the "real" mass flux values from the model. We will note these values $\widetilde{F}_{i\pm\frac{1}{2},i\pm\frac{1}{2},i\pm\frac{1}{2}}$, and $\widetilde{C}_{i,j,k}$.

With these interpolated values, and after discretization in time is also performed, Eq. 2 is not verified, and is turned into:

$$\frac{\partial \widetilde{C}_{i,j,k}}{\partial t} + \left(\widetilde{F}_{i,j,k+\frac{1}{2}} - \widetilde{F}_{i,j,k-\frac{1}{2}}\right) + \left(\widetilde{F}_{i+\frac{1}{2},j,k} - \widetilde{F}_{i-\frac{1}{2},j,k}\right) + \left(\widetilde{F}_{i,j+\frac{1}{2},k} - \widetilde{F}_{i,j-\frac{1}{2},k}\right) = -\varepsilon_{i,j,k}, \tag{6}$$

where $\varepsilon_{i,j,k}$ is a spurious matter creation term due to mass-wind inconsistencies in the interpolated density and mass-flux values from the meteorological model. $\varepsilon_{i,j,k}$ depends on the resolution of the meteorological model (which is identical for all our simulations), and on the resolution of the chemistry-transport model, so that this error term that essentially traduces divergence errors due to interpolation depends on the vertical resolution of the model. It is identical between simulations that have the exact same number of domains. Choosing interpolation strategies that reduce this error term is a promising path to mitigating excessive vertical diffusion, as discussed in Emery et al. (2011), but is not investigated here.

As discussed above, the wind in CHIMERE is normally reconstructed from the bottom to the top of the model in order to prevent mass-wind inconsistency issues.

To enforce Eq. 2, reconstructed vertical fluxes $\overline{F}_{i,j,k+\frac{1}{2}}$ are produced from the following constraints:

$$\overline{F}_{i,j,\frac{1}{2}} = 0 \tag{7a}$$

$$\overline{F}_{i,j,k+\frac{1}{2}} = \overline{F}_{i,j,k-\frac{1}{2}} + \left(\widetilde{F}_{i-\frac{1}{2},j,k} - \widetilde{F}_{i+\frac{1}{2},j,k}\right) + \left(\widetilde{F}_{i,j-\frac{1}{2},k} - \widetilde{F}_{i,j+\frac{1}{2},k}\right) - \frac{\partial \widetilde{C}_{i,j,k}}{\partial t} \tag{7b}$$

Eq. 7a gives the boundary condition to vertical mass flux reconstruction (no incoming mass flux of air comes from the ground surface). Eq. 7b ensures that, in each CTM cell and over one CTM time step, Eq. 2 is strictly verified (in the form of 7b) and Eq. 5 can be integrated using the interpolated horizontal fluxes $\widetilde{F}_{i\pm\frac{1}{2},j\pm\frac{1}{2},k}$ and the reconstructed vertical fluxes $\overline{F}_{i,j,k\pm\frac{1}{2}}$. This traditional approach will be labelled "NODIV" (for NO DIVergence) hereinafter.

In this study, we introduce and test a new approach that permits to bypass the need for a reconstructed vertical mass flux and work directly with the interpolated vertical mass fluxes $\widetilde{F}_{i,j,k+\frac{1}{2}}$ while still maintaining conservation of uniform mixing ratios. To explain this approach, we need to expand Eq. 5 as follows:

$$\begin{aligned}\frac{\partial C_{s,i,j,k}}{\partial t} &+ \left(\delta\bar{\alpha}_{i,j,k+\frac{1}{2}}\widetilde{F}_{i,j,k+\frac{1}{2}} - \delta\bar{\alpha}_{i,j,k-\frac{1}{2}}\widetilde{F}_{i,j,k-\frac{1}{2}}\right) \\ &+ \left(\delta\bar{\alpha}_{i+\frac{1}{2},j,k}\widetilde{F}_{i+\frac{1}{2},j,k} - \delta\bar{\alpha}_{i-\frac{1}{2},j,k}\widetilde{F}_{i-\frac{1}{2},j,k}\right) \\ &+ \left(\delta\bar{\alpha}_{i,j+\frac{1}{2},k}\widetilde{F}_{i,j+\frac{1}{2},k} - \delta\bar{\alpha}_{i,j-\frac{1}{2},k}\widetilde{F}_{i,j-\frac{1}{2},k}\right) \\ &+ \alpha_{i,j,k}\left[\left(\widetilde{F}_{i,j,k+\frac{1}{2}} - \widetilde{F}_{i,j,k-\frac{1}{2}}\right) + \left(\widetilde{F}_{i+\frac{1}{2},j,k} - \widetilde{F}_{i-\frac{1}{2},j,k}\right) + \left(\widetilde{F}_{i,j+\frac{1}{2},k} - \widetilde{F}_{i,j-\frac{1}{2},k}\right)\right] = 0,\end{aligned} \tag{8}$$

where $\delta\bar{\alpha}_{i,j,k+\frac{1}{2}} = \bar{\alpha}_{i,j,k+\frac{1}{2}} - \alpha_{i,j,k}$, and analogous definitions for the other $\delta\bar{\alpha}$ terms. Injecting Eq. 6 into Eq. 8 we obtain:

$$\begin{aligned}\frac{\partial \alpha_{s,i,j,k}\widetilde{C}_{i,j,k}}{\partial t} &+ \left(\delta\bar{\alpha}_{i,j,k+\frac{1}{2}}\widetilde{F}_{i,j,k+\frac{1}{2}} - \delta\bar{\alpha}_{i,j,k-\frac{1}{2}}\widetilde{F}_{i,j,k-\frac{1}{2}}\right) \\ &+ \left(\delta\bar{\alpha}_{i+\frac{1}{2},j,k}\widetilde{F}_{i+\frac{1}{2},j,k} - \delta\bar{\alpha}_{i-\frac{1}{2},j,k}\widetilde{F}_{i-\frac{1}{2},j,k}\right) \\ &+ \left(\delta\bar{\alpha}_{i,j+\frac{1}{2},k}\widetilde{F}_{i,j+\frac{1}{2},k} - \delta\bar{\alpha}_{i,j-\frac{1}{2},k}\widetilde{F}_{i,j-\frac{1}{2},k}\right) \\ &- \alpha_{s,i,j,k}\left[\frac{\partial \widetilde{C}_{i,j,k}}{\partial t} + \varepsilon_{i,j,k}\right] = 0\end{aligned} \tag{9}$$

After simplification:

$$\widetilde{C}_{i,j,k}\frac{\partial \alpha_{s,i,j,k}}{\partial t}+\left(\delta\bar{\alpha}_{i,j,k+\frac{1}{2}}\widetilde{F}_{i,j,k+\frac{1}{2}}-\delta\bar{\alpha}_{i,j,k-\frac{1}{2}}\widetilde{F}_{i,j,k-\frac{1}{2}}\right) \tag{10}$$
$$+\left(\delta\bar{\alpha}_{i+\frac{1}{2},j,k}\widetilde{F}_{i+\frac{1}{2},j,k}-\delta\bar{\alpha}_{i-\frac{1}{2},j,k}\widetilde{F}_{i-\frac{1}{2},j,k}\right)$$
$$+\left(\delta\bar{\alpha}_{i,j+\frac{1}{2},k}\widetilde{F}_{i,j+\frac{1}{2},k}-\delta\bar{\alpha}_{i,j-\frac{1}{2},k}\widetilde{F}_{i,j-\frac{1}{2},k}\right)$$
$$-\alpha_{s,i,j,k}\varepsilon_{i,j,k}=0$$

From Eq. 10, it can be observed that if the mixing ratio $\alpha_{i,j,k}=\frac{C_{s,i,j,k}}{\widetilde{C}_{i,j,k}}$ is initially uniform, then all the $\delta\bar{\alpha}$ terms vanish, and mixing ratio uniformity will be maintained after integrating Eq. 8 if, and only if, the mass-wind inconsistency term $\varepsilon_{i,j,k}$ is zero. This is already well-known but with this formulation we can obtain a modified version of Eq. 5 that will enforce mixing ratio preservation even if the mass-wind inconsistency term $\varepsilon_{i,j,k}$ is not zero:

$$\frac{\partial C_{s,i,j,k}}{\partial t}+\left(\bar{\alpha}_{i,j,k+\frac{1}{2}}\widetilde{F}_{i,j,k+\frac{1}{2}}-\bar{\alpha}_{i,j,k-\frac{1}{2}}\widetilde{F}_{i,j,k-\frac{1}{2}}\right) \tag{11}$$
$$+\left(\bar{\alpha}_{i+\frac{1}{2},j,k}\widetilde{F}_{i+\frac{1}{2},j,k}-\bar{\alpha}_{i-\frac{1}{2},j,k}F_{i-\frac{1}{2},j,k}\right)$$
$$+\left(\bar{\alpha}_{i,j+\frac{1}{2},k}\widetilde{F}_{i,j+\frac{1}{2},k}-\bar{\alpha}_{i,j-\frac{1}{2},k}\widetilde{F}_{i,j-\frac{1}{2},k}\right)+\mathbf{C_{s,i,j,k}}\frac{\varepsilon_{\mathbf{i,j,k}}}{\widetilde{\mathbf{C}}_{\mathbf{i,j,k}}}=0$$

Eq. 11 will be solved in the simulation labeled WRFW, with mass fluxes directly interpolated from the meteorological model winds in the three directions. It must be noted that mass conservation is not enforced by this equation: the additional term $\mathbf{C_{s,i,j,k}}\frac{\varepsilon_{\mathbf{i,j,k}}}{\widetilde{\mathbf{C}}_{\mathbf{i,j,k}}}$ is an artificial mass production/loss term that breaks the conservation of total mass of species s over the entire domain. If we summarize this part, the NODIV simulation (classical approach) enforces tracer mass conservation and tracer mixing ratio conservation. This is obtained to the expense of irrealistic vertical transport, since mass-wind consistency is, in this approach, enforced by artificially modifying the vertical mass fluxes. However, this reconstructed wind is significantly different from WRF input data while reaching the upper troposphere (Figure S1 in supplements), and this approach induces excessive transport across tropopause. Vertical wind distribution comparisons between WRFW and NODIV strategies (Figure S1) show that more vertical diffusion is expected in the NODIV strategy in the upper troposphere. The WRFW approach that we propose here, on the other hand, permits mixing ratio conservation and the use of realistic vertical mass fluxes, to the expense of mass conservation. While non-conservation of mass is obviously a significant drawback for a transport strategy, we will quantify this problem of non-conservation of mass, as well as the problems introduced by artificial reconstruction of vertical mass fluxes in the representation of vertical transport in the NODIV approach (Figure 3).

2.2.2 Vertical advection scheme

After discretizing the advection equation for species s in the form of Eq. 5, the point of the vertical transport scheme is to estimate the reconstructed mixing ratios $\bar{\alpha}_{i,j,k+\frac{1}{2}}$, for k varying between 1 and the number of vertical levels nz. The most simple way of doing so is the Godunov donor-cell scheme, simply evaluating $\bar{\alpha}_{s,i,j,k+\frac{1}{2}}$ as:

$$\bar{\alpha}_{s,i,j,k+\frac{1}{2}} = \alpha_{s,i,j,k} \quad \text{if } \mathrm{F_{i,j,k+\frac{1}{2}}} > 0 \tag{12}$$

$$\bar{\alpha}_{s,i,j,k+\frac{1}{2}} = \alpha_{s,i,j,k+1} \text{ if } \mathrm{F_{i,j,k+\frac{1}{2}}} < 0 \tag{13}$$

This order-1 scheme is mass-conservative but extremely diffusive. It is therefore important to find more accurate ways to estimate $\bar{\alpha}_{s,i,j,k+\frac{1}{2}}$.

The Van Leer (1977) scheme

The second-order slope-limited scheme of Van Leer (1977) brought to our notations yields the following expression of $\bar{\alpha}_{s,k+\frac{1}{2}}$ (for $F_{i,j,k+\frac{1}{2}} > 0$).

$$\bar{\alpha}_{s,k+\frac{1}{2}} = \alpha_{s,k} + \frac{1-\nu}{2}\mathrm{sign}\left(\alpha_{s,k+1} - \alpha_{s,k}\right)\mathrm{Min}\left(\frac{1}{2}\left|\alpha_{s,k+1} - \alpha_{s,k-1}\right|, 2\left|\alpha_{s,k+1} - \alpha_{s,k}\right|, 2\left|\alpha_{s,k} - \alpha_{s,k-1}\right|\right), \tag{14}$$

where $\nu = \frac{F_{i,j,k+\frac{1}{2}}}{\rho_{i,j,k} V_{i,j,k}}$ is the Courant number for the donor cell i,j,k, $V_{i,j,k}$ being its volume: if $\nu > 1$, then more mass leaves the cell than the mass that was initially present and the Courant-Friedrichs-Lewy condition is violated, yielding numerical instability. ~~If $\alpha_{s,k}$ is~~ Eq. 15 is not applied in the case of a local extremum ~~of mixing ratio~~ ($(\alpha_{s,k} - \alpha_{s,k-1})(\alpha_{s,k+1} - \alpha_{s,k}) \leq 0$)~~, no interpolation is performed~~. In this case, $\bar{\alpha}_{s,k+\frac{1}{2}} = \alpha_{s,k}$ is imposed and the scheme falls back to the simple Godunov donor-cell formulation (Eq. 12). This order-2 scheme has been used for decades in chemistry-transport modelling, being a good tradeoff between reasonably weak diffusion, at least compared to more simple schemes such as the Godunov donor-cell scheme, ~~and small computational burden compared to~~ computationally cheaper than higher-order schemes such as the Piecewise Parabolic Method (Colella and Woodward, 1984).

The Després and Lagoutière (1999) scheme

The scheme of Després and Lagoutière (1999) is defined by their equations 2 to 4. If $F_{i,j,k+\frac{1}{2}} > 0$, these equations brought to our notations, adapted to the flux form of Eq.5 and ignoring the i,j indices to shorten the expression, give:

$$\bar{\alpha}_{s,k+\frac{1}{2}} = \alpha_{s,k} + \frac{1-\nu}{2}\mathrm{Max}\left[0, \mathrm{Min}\left(\frac{2}{\nu}\frac{\alpha_{s,k} - \alpha_{s,k-1}}{\alpha_{s,k+1} - \alpha_{s,k}}, \frac{2}{1-\nu}\right)\right] \times \left(\alpha_{s,k+1} - \alpha_{s,k}\right), \tag{15}$$

with the same notations as for the Van Leer (1977) scheme (above). As above, ~~if~~ Eq. 15 is not applied in the case of a local extremum ($(\alpha_{s,k} - \alpha_{s,k-1})(\alpha_{s,k+1} - \alpha_{s,k}) \leq 0$)~~, no interpolation is performed~~. In this case, $\bar{\alpha}_{s,k+\frac{1}{2}} = \alpha_{s,k}$ is imposed and the scheme falls back to the simple Godunov donor-cell formulation (Eq. 12). As stated by its authors, this scheme is antidiffusive. Unlike other schemes such as the Van Leer (1977) scheme described above, two unusual choices have been made by the authors in order to minimize diffusion by the advection scheme:

- Their scheme is accurate only to the first order

Table 1. List of the various model parameters tested, allowing to perform a total of 12 distinct simulations.

Vertical levels	Vertical transport scheme	Vertical wind strategy
20	VL	NODIV
50	DL	WRFW
99		

– The scheme is linearly unstable, but non-linearly stable (their Theorem 1)

The idea of the authors has been to make the interpolated value $\bar{\alpha}_{s,k+\frac{1}{2}}$ as close as possible to the downstream value ($\alpha_{s,k+1}$ if the flux is upward). This property is desirable because it is the key property in order to reduce numerical diffusion as much as mathematically possible while still maintaining the scheme stability. The authors present 1d case-studies with their scheme obtaining extremely interesting results: fields that are initially concentrated on one single cell do not occupy more than 3 cells even after a long advection time (their ~~Fig.~~ Figure 2), sharp gradients are very well preserved (their ~~Fig.~~ Figure 1), and, more unexpectedly due to its antidiffusive character, the scheme also performs well in maintaining the shape of concentration fields with an initially smooth concentration gradient. After extensive testing, these authors also suggest (their Conjecture 1) that convergence of the simulated values towards exact values occur even if the time step is reduced before the space step: in simpler terms, this means that the scheme performs very well even at small CFL values, a property that is not shared by most advection schemes.

2.2.3 Model parameters tested

The various possible parameter combinations between the vertical flux (NODIV for reconstructed vertical fluxes, WRFW for interpolated vertical mass flux), the vertical transport scheme (VL for Van Leer (1977), DL for Després and Lagoutière (1999)) and the number of vertical levels (20, 50, 99) are summarized in Table 1. Following all the possible combinations between these parameters, 12 simulations have been performed.

2.3 SO_2 emissions from the March 18 2012 eruption of Mount Etna

The time and altitude profiles for injection of SO_2 into the atmosphere (Table 2) have been obtained using SO_2 flux measurement data from the ground-based DOAS FLAME (Differential Optical Absorption Spectroscopy FLux Automatic MEasurements) scanning network (e.g. Salerno et al., 2018). This method accurately measures SO_2 fluxes during passive degassing and effusive and explosive eruptive activity using a plume height inverted by an empirical relationship between plume height and wind speed (Salerno et al., 2009). In explosive paroxysmal events, as in the case in this study, the plume is ejected to higher altitudes and this linear height-wind relationship can not be used~~and mass~~. Mass flux is retrieved in post-processing using the plume height estimated by visual camera and/or satellite retrieval.

Table 2. SO_2 hourly flux ($kg.s^{-1}$) estimates used as input for the CHIMERE model.

date, time	SO_2 flux ($kg.s^{-1}$)	injection height (m.a.s.l)
18/03/2012, 06 UTC	12.36	4500
18/03/2012, 07 UTC	9.42	6500
18/03/2012, 08 UTC	466.87	12000
18/03/2012, 09 UTC	276.09	12000
18/03/2012, 10 UTC	31.95	6000
18/03/2012, 11 UTC	3.73	4500
18/03/2012, 12 UTC	4.24	4500
18/03/2012, 13 UTC	5.05	4500
18/03/2012, 14 UTC	4.12	4500
18/03/2012, 15 UTC	4.38	4500

Table 3. IASI and OMI soundings list. $\lambda_{\mathrm{OBS},i}$ (longitude) and $\Phi_{\mathrm{OBS},i}$ (latitude) represent plume's column with the highest SO_2 content coordinates. $\lambda_{\mathrm{thr},i}$ is the limit longitude that has been set as limit between the Eastern and Western plumes in section 3.4.~~Logscale is used to better visualized CHIMERE simulations, but values under 3e15 (~0.1DU) are below satellite detection limits.~~

date, time	Instrument	sounding number, i	$\lambda_{\mathrm{OBS},i}$	$\Phi_{\mathrm{OBS},i}$	$\lambda_{\mathrm{thr},i}$	Figure
18/03/2012, 12 UTC	OMI	1	$17°07'$	$37°52'$		
18/03/2012, 17 UTC	IASI	2	$20°23'$	$37°08'$	$17°45'$	Figure S2
19/03/2012, 06 UTC	IASI	3	$27°23'$	$34°15'$	$19°30'$	Figure 2
19/03/2012, 12 UTC	OMI	4	$29°07'$	$33°37'$		Figure 2
19/03/2012, 17 UTC	IASI	5	$34°23'$	$33°23'$	$21°30'$	Figure S2
20/03/2012, 12 UTC	OMI	6	$46°37'$	$34°37'$		

On March 18 2012, between 06 UTC and 15 UTC, a total SO_2 emission of 2.94 kt has been reported by this method. 91 % of this mass has been released within 2 hours around 12 km of altitude. In CHIMERE, emissions have been distributed into a single model cell based on altitude injection. Two alternates cases have been tested, considering -1 km and +1 km for all of the injection heights defined in Table 2.

2.4 IASI and OMI instruments

To evaluate the numerical parameters tested in our simulations, satellite based information were used to evaluate the SO_2 plume transport and vertical distribution. SO_2 column observations are provided by the Infrared Atmospheric Sounding Interferometer

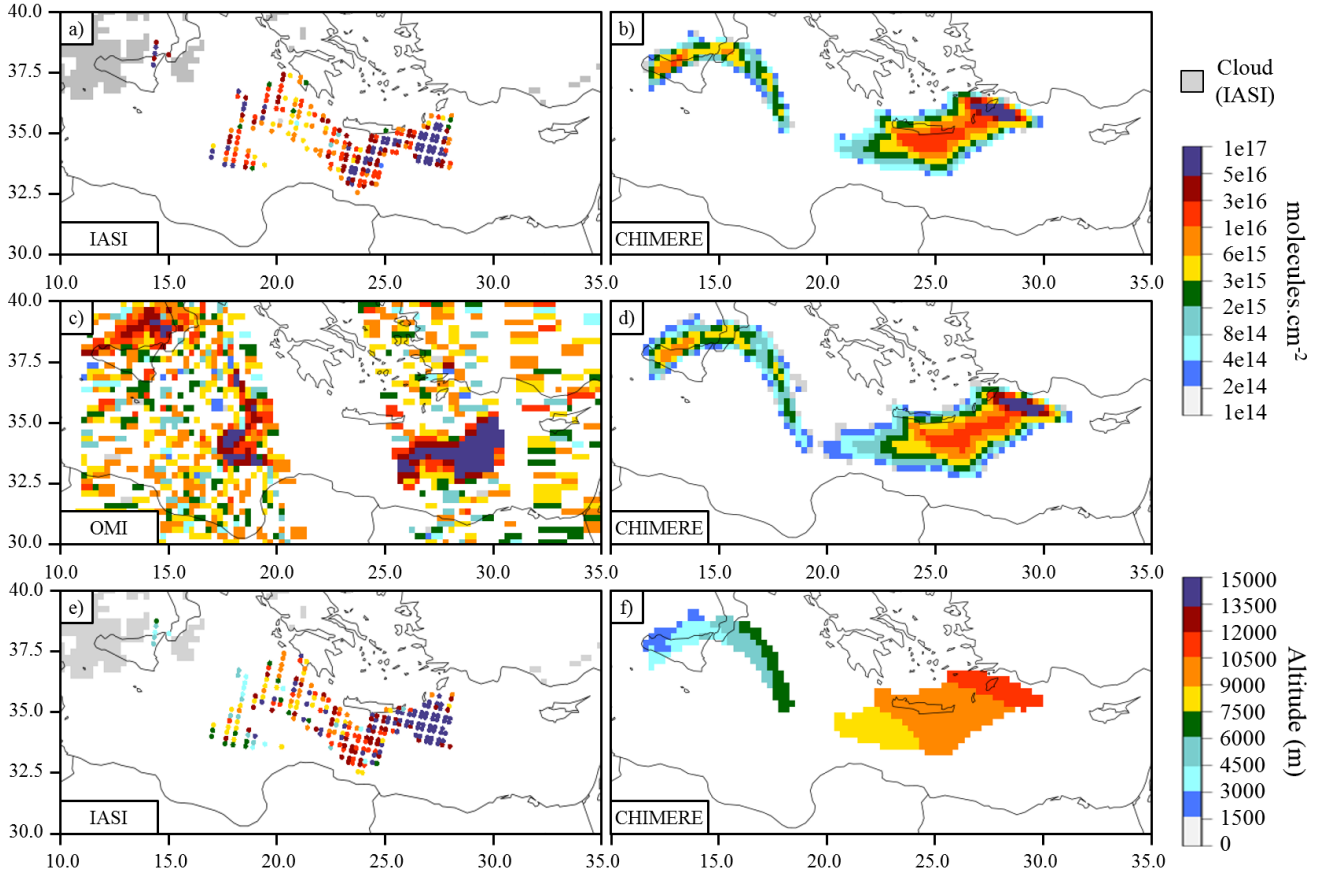

Figure 2. IASI SO_2 plume (a), OMI SO_2 plume (c), IASI and OMI soundings respectively for March 19 2012 06AM and 12AM UTC (3 and 4 in Table 3). CHIMERE SO_2 plume (b and d) in $\mathrm{molecules.cm^{-2}}$ corresponding to IASI and OMI soundings. IASI SO_2 altitude (e) and CHIMERE SO_2 maximum concentrations' altitude (f) in meters March 19 2012 06AM UTC. In this example, CHIMERE simulation WRFW-DL-20 is displayed. CHIMERE and OMI data are represented with OMI's $0.25° \times 0.25°$ resolution grid. Clouds are based on Advanced Very High Resolution Radiometer (AVHRR) data for IASI. Logscale is used to better visualized CHIMERE simulations, but values under 3e15 (~0.1DU) are below satellite detection limits.

instrument (IASI) on board the Metop-A European satellite and the Ozone Monitoring Instrument (OMI) on board the Aura NASA satellite (Levelt et al., 2006; McCormick et al., 2013). IASI instrument is operating between 3.7 and 15.5 µm, including SO_2 ν_1 (around 8.7 µm) and ν_3 (7.3 µm) bands (Carboni et al., 2012). IASI scheme (Carboni et al., 2012, 2016) provides SO_2 total column content and ~~altitude and it~~ plume altitude. This product is shown in Figure 2 together with OMI SO_2 columns and CHIMERE outputs. In our analysis we used IASI retrievals from March 18, 17UTC (~~Fig.~~Figure S2), March 19, 06UTC (~~Fig.~~Figure 2) and March 19, 17UTC (~~Fig.~~Figure S3). OMI data are obtained from the NASA GIOVANNI platform[2]. OMI

[2]https://giovanni.gsfc.nasa.gov/giovanni/, last consulted 08/29/19. Krotkov et al.

Data are provided with a $0.25° \times 0.25°$ resolution and a daily coverage, at 12AM UTC for 18^{th}, 19^{th} and 20^{th} of March over the studied area. All instruments soundings are resumed in Table 3.

3 Results and Discussion

3.1 ~~The impact~~ Impact of ~~the~~ injection altitude on plume ~~'s~~ transport

Alternative injection height scenarios have been tested, either lifting or lowering the injection height at all times by 1 km, thereby lifting maximum injection heights up to 13 km (res. lowering it down to 11 km) instead of 12 km in the reference simulation. These tests have shown that plume trajectories are strongly sensitive to this parameter (~~Fig.~~Figure 1), which is an effect of wind shear. For each satellite sounding, the coordinates of the model column with the strongest vertically integrated SO_2 content ($\mathrm{molecules_{SO_2}.cm^{-2}}$) have been selected and considered as SO_2 plume centroids. Doing so with the available 3 IASI soundings and 3 OMI soundings gives 6 points on the satellite-retrieved Etna plume trajectory, ranging from Sicily to Western Iran. The IASI/OMI centroids and constructed plume trajectory are displayed in black on Figure 4.

Simulations and satellite plumes initial position do not correspond to Etna location because OMI first sounding is at 12 UTC on March 18, 6 hours after the beginning of the eruption. Compared to the trajectory reconstituted from OMI and IASI observations, the plume injected at 11 km seems to be transported too far towards the South, while the plume injected at 13 km appears to be shifted to the North compared to observations. This observation is largely ~~independant~~ independent of the model parameters (NODIV-VL-99 and WRFW-DL-99 are shown on ~~Fig.~~Figure 1), suggesting that the configuration with a maximum injection height at $12\,\mathrm{km}$ is the best configuration. Therefore, only this choice for injection height will be retained for the rest of the study.

In addition, sensitivity to injection vertical profile has been investigated with 3 options:

- Injection to a unique altitude
- Injection with a full width at half maximum of 100 m (Boichu et al., 2015)
- Injection with a full width at half maximum of 300 m

The tests have been conducted on 20, 50 and 99 vertical levels resolution. These sensitivity tests have shown little differences between the various cases, even in 99 vertical levels resolution, with plumes close trajectories and vertical diffusion. Injection to a unique altitude - consequently in a unique cell - has been conserved and used to perform and evaluate the vertical diffusion strategies.

3.2 Mass conservation

Figure 3 shows the evolution of the total mass of tracer inside the simulation domain as a function of time. Several features from this figures need to be commented.

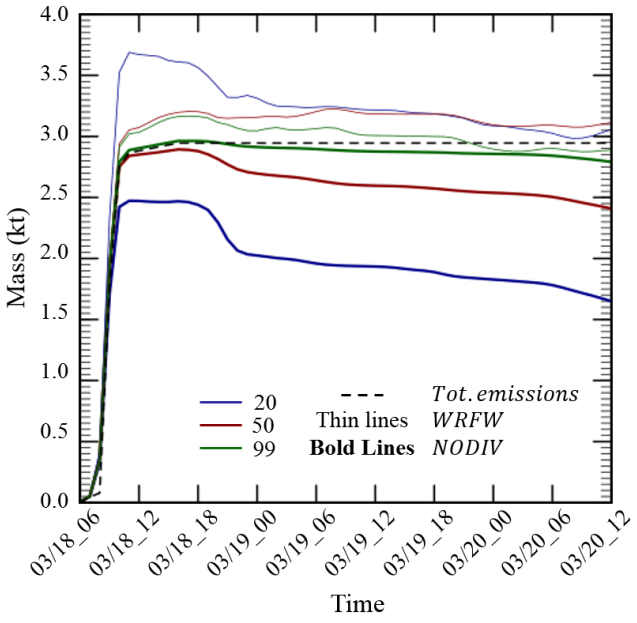

Figure 3. SO_2 mass evolution in model domain (kilotons). Line color indicates the vertical levels configuration, thickness indicates the vertical wind strategy considered. Dotted line represents the cumulated SO_2 mass emitted during Etna volcanic Eruption.

In the simulations with the reconstituted non-divergent wind field, substantial mass leak through the top of model can be observed as soon as the injection starts in the 20-level simulation (in which injection is done in the highest model level): the mass of tracer present in the domain never exceeds 85% of the emitted mass. For the simulation with 50 vertical levels, this phenomenon is also visible. Another strong episode of mass leak through model top occurs in the simulations with 20 and 50 vertical levels and with reconstructed wind fields from March 18, 18UTC to March 19, 00UTC. This episodes causes an additional drop in tracer mass of 20% in the simulation with 20 levels, 5% in the simulation with 50 vertical levels. This episode of leak also affects the simulation with 20 vertical levels and with interpolated wind fields, reducing tracer mass concentration by about 10% from March 18, 18UTC to March 19, 00UTC. In these three simulations (20 and 50 levels with non-divergent winds, 20 levels with interpolated winds), a continuous decreasing trend in tracer mass is observed throughout the simulation. This drop is directly attributable to leak through model top since the tracer plume is far away from the horizontal boundaries of the domain.

As it could be expected, the simulations with the WRFW wind strategy, due to the additional term in Eq. 11, ~~does~~ do not enforce mass conservation. In theory, the additional term, designed to ensure mixing ratio conservation in spite of mass-wind inconsistencies, can result into either an artificial increase or an artificial decrease in simulated tracer mass. In the three simulations that are shown on ~~Fig.~~Figure 3, the amount of tracer present in the domain just after the end of the eruption overshoots the expected mass, by 20% in the simulation ~~in the simulation~~ with 20 vertical levels, 10% in the two simulations with a larger number of levels. ~~In the later stages of plume evolution~~ No physical process can explain this overshoot, and it is

directly attributable to the choice of lifting the mass conservation constraint in the formulation of transport in order to permit the use of a realistic wind field. If we take March 19, 00UTC as a reference time at which the eruption is terminated, the first strong event of leak through model top is terminated as well, we can observe that the mass evolution in all three WRFW simulations undergoes small variations from one hour to the next but stay confined in very narrow ranges : 3.3 to 3 kt for the simulation with 20 vertical levels, with a decreasing trend attributable to leakage through model top, 3.1 to 3.25 for the simulation with 50 levels and 2.9 to 3.1 kt for the simulation with 99 vertical levels. The fact that these variations in total mass become marginal in this latter part of plume advection, when the plume is spread over a ~~larger area the spurious evolutions in tracer mass become weaker, less than 5%~~large geographic areas reflect the fact that numerical errors in the evaluation of divergence mechanically tend to compensate each other between neighbouring cells so that their global impact on a plume that is dispersed over many cells is small.

3.3 Horizontal transport evaluation with OMI and IASI instruments

In this section we aim to determine how the various parameters tested (Table 1) have influenced plume trajectory. Plume trajectory from simulations have been constructed following the same methodology as described above for satellite data, using the corresponding satellite sounding time step and retaining the coordinates of the model column with the strongest vertically integrated SO_2 content. The trajectories of all 12 ~~different simulations-based trajectories~~ simulations are shown in Figure 4a, ~~so to identify~~ with a color-code aimed at highilghting the impact of vertical levels number on the diffusion~~(20 levels: shades of blue, 50 levels: shades of red, 99 levels: shades of green)~~. Figure 4b allows to compare the influence of the vertical transport schemes (VL or DL), and finally Figure 4c allows to compare the various vertical wind strategies (NODIV or WRFW) influence.

It can be observed that for the various 20 vertical levels simulations, no significant differences between the vertical transport schemes nor vertical wind strategy are found, except for NODIV-VL-20 simulation which strongly diverges and split into 2 different plumes at OMI's last sounding. For 50 and 99 vertical levels simulations, more differences are found, mainly controlled by the choice of vertical transport schemes (VL or DL). As for NODIV-VL-20, NODIV-VL-50 simulation presents for OMI's last sounding a split in two distinct SO_2 plumes.

To conduct a ~~quantitative~~ more quantitative and synthetic analysis of the deviation between observations and model outputs, the geographic distance between satellite observation centroids and simulations centroids has been calculated for every sounding. This calculation provides for each simulation a satellite - model differences time series. Then, to better estimate the impact of the tested parameters, gap means have been calculated according to simulations ~~options~~ parameters to evaluate separately the impact of each parameter choice on the accuracy of ~~the plume~~ plume simulation. Results are displayed in Figure 5a. A ~~global~~ general mean value for each time series is calculated and added on Figure 5a, last boxes. As expected, gaps between satellite and model centroids generally increase with time.

It can be seen that the DL vertical scheme has better agreement with the observations than the VL vertical scheme, with respectively a mean gap of 189 km and 316 km - with NODIV wind strategy option fixed. The WRFW wind strategy also

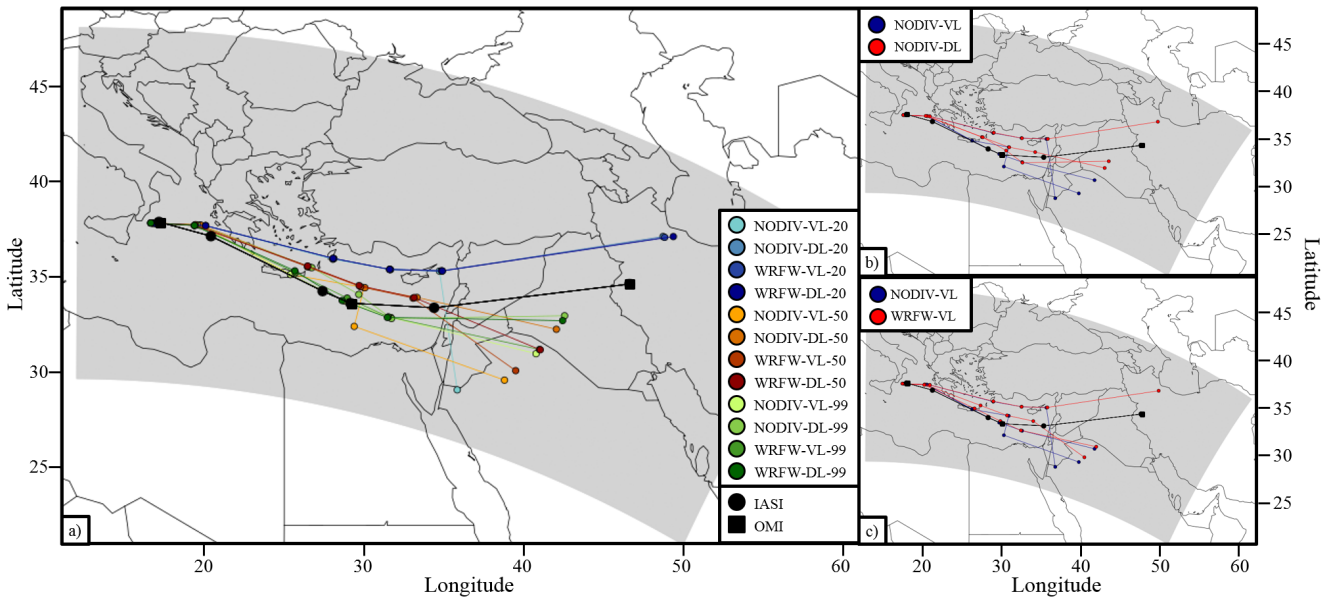

Figure 4. Etna volcanic plume transport over the Mediterranean sea after the March 18 2012 eruption. Satellite trajectory (black line) built combining IASI and OMI instruments information. a) Transport for all simulations, b) plume transport highlighted according to vertical scheme, c) plume transport highlighted according to vertical wind strategy. The points along the trajectories correspond to those listed in Table 3.

shows better agreement with soundings than the NODIV strategy, with a mean gap of respectively 230 km and 316 km - with VL vertical scheme fixed.

To complete the centroids-gap analysis, agreement between satellite measurements and model simulations in the zonal and meridional displacements of the centroids has been calculated, as expressed in Equation 16 for a given simulation (SIM):

$$\Delta_{(i,i-1),\mathrm{SIM}}(km) = \mathrm{R}\sqrt{\cos^2\Phi\left(\Delta\lambda_{\mathrm{SIM},(i,i-1)} - \Delta\lambda_{\mathrm{OBS},(i,i-1)}\right)^2 + \left(\Delta\Phi_{\mathrm{OBS},(i,i-1)} - \Delta\Phi_{\mathrm{SIM},(i,i-1)}\right)^2}, \quad (16)$$

where

$$\Delta\lambda_{\mathrm{SIM},(i,i-1)} = \lambda_{\mathrm{SIM},i} - \lambda_{\mathrm{SIM},i-1}, \text{ and}$$
$$\Delta\lambda_{\mathrm{OBS},(i,i-1)} = \lambda_{\mathrm{OBS},i} - \lambda_{\mathrm{OBS},i-1}.$$

~~where the~~ i ~~index~~ refers to sounding numbers (Table 3), $\lambda_{\mathrm{OBS},i}$ and $\Phi_{\mathrm{OBS},i}$ refer to the geographic coordinates of the observed centroid for sounding i at time t_i (Table 3), $\lambda_{\mathrm{SIM},i}$ and $\Phi_{\mathrm{SIM},i}$ to the coordinates of the ~~centroid simulated~~ simulated centroid, and R is the Earth radius. In this case we focus on the displacement of the plume between two successive observation

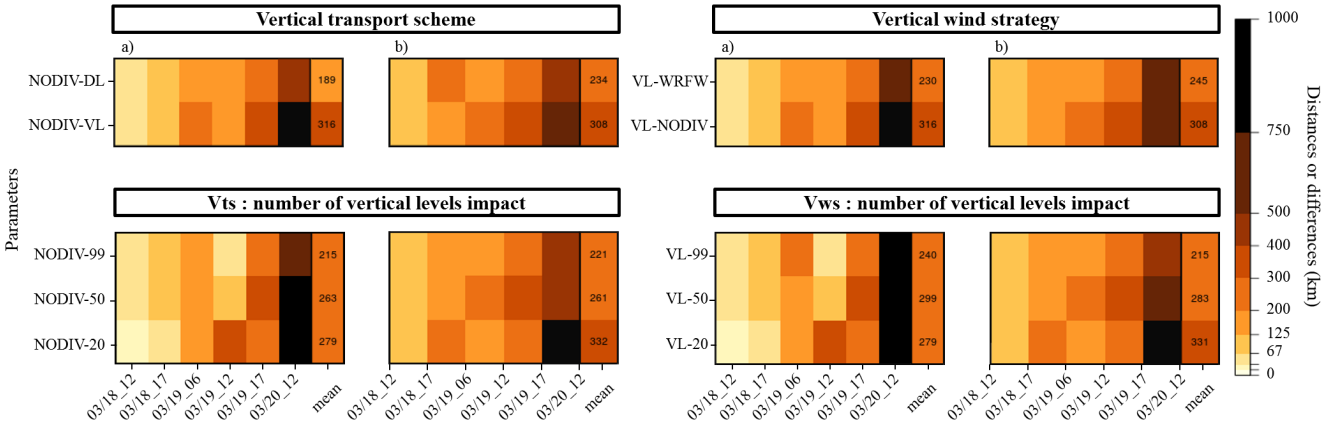

Figure 5. Left) Vertical transport scheme impact, Right) Vertical wind strategy impact. a) Gap between satellites and CHIMERE SO_2 plume centroids. b) Differences between SO_2 plume centroids trajectories. To produce this figure, differences (in km) between model and satellite plumes centroids are calculated for each simulation, then the impact of each parameter is evaluated by calculating the mean between simulation-satellite differences. For instance, "NODIV-DL" (1^{st} line, left column) is the mean between "NODIV-DL-20", "NODIV-DL-50", "NODIV-DL-99". "NODIV-99" (3^{rd} line, left column) is the mean between "NODIV-DL-99" and "NODIV-VL-99".

points. The intention of Eq. 16 is to build an index that not only qualifies the distance between the observed and modelled trajectories, but also the realism of the displacements followed between two successive satellite snapshots, giving penalties to simulations which would oscillate erratically around the observed trajectory and bonuses to simulations that would follow a realistic trajectory, but slightly shifted towards either side. Results are displayed on Figure 5b, and again mean value for each time series has been calculated and displayed on Figure 5b last boxes. It can be observed, as in the previous indicator case, the DL vertical scheme and WRFW vertical wind strategy have brought better results than the respectively opposed VL and NODIV parameters.

It also appears clearly for both criteria that the 99 vertical levels option shows the best results to both, centroids position and trajectory comparisons to the satellite than the 50 or 20 vertical levels options.

3.4 Comparison of the simulated plume vertical structure with IASI-retrieved structure

IASI observations also provide the estimated altitude of the SO_2 plume for each pixel with a valid SO_2 retrieval (Figure 2e), along with the corresponding uncertainty. For each of the three available IASI soundings (Numbers 2, 3 and 5 in Table 3), we have extracted the plume altitude and its associated uncertainty for the pixel with the highest content of SO_2. Comparison of this plume altitude with the same calculation made on the plume simulated by CHIMERE is shown on Figure S4 (in supplements). It can be observed that for the IASI first available sounding, soon after the Etna eruption, concentration maximum altitude for CHIMERE is consistent with IASI altitude and is found within IASI uncertainties ($12\,100\,\mathrm{m} \pm 900\,\mathrm{m}$): Along with the trajectories shown on ~~Fig.~~ Figure 1, this is an indication that the highest emission altitude at $12\,\mathrm{km}$ in Tab. 2 is realistic.

In the IASI dataset, a bimodal altitude distribution is observed, indicating ~~the~~ coexistence of two separated sub-plumes during this eruption: one located to the East at higher altitude, another one located to the West at lower altitude (Figure 2), which has also been observed in AEROIASI-sulphates soundings in (Sellitto et al., 2017; Guermazi et al., 2019). This separation is due to the sharp separation between emissions at very high altitudes ($\simeq 12\,\mathrm{km}$) and emissions below $\simeq 7,5\,km$ (Tab. 2) and to the fact that at the Etna latitude wind shear is generally strong with steady westerly winds in the higher troposphere and more variable winds in the lower troposphere. Since most of SO_2 is emitted around $\simeq 12\,\mathrm{km}$ (Table 2), most of SO_2 mass is found in the Eastern plume. From each available IASI observation of the plume (soundings 2, 3 and 5 in Tab. 2), a transition longitude that separates the western plume from the eastern plume has been identified. These longitudes are given in Tab. 2 and can be compared to Figures S2 and S3. The same longitudes have been used to ~~split the CHIMERE simulated plumes between a~~ separate the Eastern and Western plume in the CHIMERE simulations. Figure 6 compares the altitude distribution between the CHIMERE simulations and IASI retrievals - 20 vertical levels simulations have been removed, because ~~of~~ the coarse altitude resolution does not permit a useful representation of the maximum concentration's altitude distribution (see Figure S4, in supplements). ~~IASI data presents a broader vertical distribution than CHIMERE simulations, meaning that the plume height variability is stronger in the IASI retrievals than in the CHIMERE data. The highest values of plume altitude are significantly higher in IASI than in simulations.~~ Altitude distribution median values are extremely close for both plumes between CHIMERE simulations and IASI soundings. The various parameters tested have not significantly changed the altitude distribution median but have impacted altitude distributions' widths, which have been slightly tightened for 99 vertical levels, DL vertical transport scheme and WRFW vertical wind strategy. ~~The fact that the modelled distributions of the plume altitudes are always much tighter than observed distribution can be attributed to a potential underestimation of plume variability by the model~~

The IASI dataset also provides error-range estimates along with the retrieved plume altitude. These error-range estimates have a median of around 1000 m in the western plume and ~~/or to the large uncertainties in IASI estimates for plumealtitude~~5000 m in the eastern plume, which is much higher aloft. These uncertainties help to understand the wide distribution obtained from satellite. It is also worth noting that this dataset provides plume altitude but does not provide an information on plume thickness. Therefore, comparison between the left and right panels in Figure 2 does not represent the compared plume thickness between model and observation, but the compared variability of plume height. Unfortunately, due to the relatively large ucertainties affecting the retrieved altitudes, no conclusion can be made on this point either. With all these limitations, Figure 2 prove that model simulations represent the general structure of the plume, with an elevated eastern plume and a low western plume, and that the median altitudes of both these plumes are very comparable to the median of the satellite-provided altitudes.

3.5 Impact of model configuration on SO_2 vertical diffusion

To evaluate directly the impact of the various model configurations on SO_2 vertical diffusion, time evolution of the SO_2 vertical profile for the model column with the strongest SO_2 content at each hourly model output steps are shown on ~~Fig.~~Figure 7, showing that:

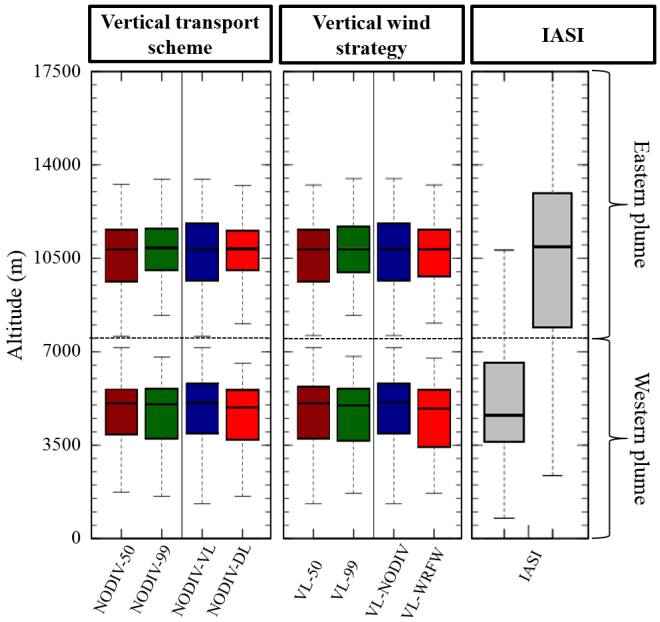

Figure 6. SO_2 plume maximum concentration's altitude distributions for IASI measurements and CHIMERE model simulations for the different configurations tested. Brackets correspond to distribution's 10^{th} and 90^{th} percentiles

- 20 vertical levels are clearly insufficient to reproduce correctly even the main features of the plume advection in this case: no evolution of the plume altitude can be seen at such a coarse vertical resolution, and the plume seems to be strongly leaking through the top of model, which is not the case with 50 or 99 vertical levels

- The simulation that diffuses less the plume is the WRFW-DL-99

- Using an antidiffusive advection scheme permits to reduce diffusion almost as strongly as increasing the number of levels: for example, simulation NODIV-DL-50 preserves the maximum concentration of SO_2 in the plume and the thin plume structure as well as simulation NODIV-VL-99, with a calculation cost divided by two due to the reduced number of vertical levels. Therefore, the use of an antidiffusive advection scheme is a very attractive means of reducing numerical diffusion on in the vertical direction without increasing the computational cost of the simulation.

- Using the realistic vertical wind WRFW instead of the vertically reconstructed NODIV wind also reduces numerical diffusion and avoids intermittent leaks of the tracer through the upper model boundary, as can be seen by comparison between the NODIV-VL-20 and WRFW-VL-20 simulations for example.

- Combining an antidiffusive advection scheme, the use of real vertical wind and the largest number of levels systematically permit to reduce plume diffusion. Qualitatively, the impact of the antidiffusive transport scheme on reducing vertical diffusion seems to be more prononced than that of using real vertical winds instead of reconstructed ones: in

~~Fig.~~ Figure 7: plumes on the third row of ~~Fig.~~ Figure 7, with the Després and Lagoutière (1999) scheme and reconstructed vertical winds, are systematically less diffused than their counterpart on the second row with the Van Leer (1977) scheme and realistic vertical winds.

– Examination of the 4 simulations with 99 vertical levels shows that the Després and Lagoutière (1999) preserves much higher maximal concentrations in the plume: at the last simulation step, both simulations with the DL99 scheme exhibit maximum SO_2 concentrations in the 75-250 ppb range, while both simulations with Van Leer (1977) have maximal concentrations in the 10-25 ppb range little more than 48 hours after the eruption, and all other things being equal, choosing the Després and Lagoutière (1999) anti-diffusive transport scheme permits the simulated concentration to be at least 4 times as strong as with the classical ~~Després and Lagoutière (1999)~~ Van Leer (1977) scheme.

3.6 Parameters impact on SO_2 dispersion

In the aim to evaluate the SO_2 overall diffusion (vertical and horizontal) following the present Etna eruption, we have compared the minimum volume in which 50 % of SO_2 mass can be found for each time step and for each simulations. Volume evolution have been represented on Figure 8a. 20 levels simulations present the highest volume occupied, and 99 levels simulations the lowest volume occupied. The simulation which restricts most the diffusion is WRFW-DL-99 one, and by opposition, the one which contains less efficiently the plume is NODIV-VL-20.

To assess the impact of the applied vertical scheme or vertical wind strategy, the volume ratio evolution between VL and DL vertical scheme for each vertical levels number has been calculated - with the wind strategy fixed (NODIV). Likewise, the volume ratio evolution between NODIV and WRFW wind strategy for each vertical levels number has been calculated - with the vertical scheme fixed (VL). Volume ratio evolution have been summarized on Figure 8b. It appears that the DL vertical transport scheme ~~DL reduce strongly the~~ strongly reduces diffusion compared to VL, as the volume ratios $Vol_{NODIV-VL}/Vol_{NODIV-DL}$ increase with time for the three level numbers configuration. Results are less clear for the vertical wind strategy, as the volume ratios $Vol_{NODIV-VL}/Vol_{WRFW-VL}$ slightly increase in most of the cases, with a stronger effect in the 20 vertical levels case. Finally, we observe that the combination of WRFW and DL parametrisation has consequently reduced the atmospheric diffusion~~such as the occupied~~ , so that plume volume for WRFW-DL-20 is quite similar to the NODIV-VL-99 case: using a realistic vertical wind field and an antidiffusive scheme is, for this criterion, as efficient as refining the model vertical resolution by a factor of 5. ~~By extension, it has been observed thatvolcanic plumeshape has been modified by DL and WRFW parameters, reducing the surface area containing~~

As discussed in Zhuang et al. (2018); Eastham and Jacob (2017), reducing vertical diffusion has a direct impact on reducing horizontal diffusion as well. Figure S6 shows integrated SO_2 colums for six model configurations 48h after the eruption. We can observe here that, in terms of maximum value of integrated SO_2 column, WRFW-DL-50 produces a maximum value slightly stronger than NODIV-VL-99, with strikingly similar horizontal structures. Also, in spite of the fact that 20 vertical layers are clearly not sufficient to reproduce the plume, we can see that, if we take the 99-level simulations as reference points, the output of the WRFW-DL-20 is clearly better than NODIV-VL-20 in terms of horizontal structure and maximal column values,

which is visible in many aspects: orientation of the low-level plume from south-eastern Italy to the Aegean sea and north-south from the Aegean sea to eastern Libya, stronger maximal values of SO_2 columns in the main part of the plume above the Middle-East. This qualitative comparison is in line with the results of Zhuang et al. (2018); Eastham and Jacob (2017) in the fact that improving vertical resolution will substantially reduce the horizontal spread in simulated plumes as well. We have also calculated the minimum area containing more than 50 ~~% of total mass~~ % of the SO_2 mass (Figure S7), showing that the WRFW-DL simulations concentrate 50% of the plume mass in an area at least twice as small as their NODIV-VL counterparts.

~~In order to analyse atmospheric diffusion, the~~

3.7 Evaluation of SO_2 dispersion with similar vertical extension at injection

To evaluate the impact schemes and vertical resolution would have with a similar vertical extension at injection, new simulations have been conducted imposing an identical vertical distribution at the first time (spreading vertically the emited mass over the same thickness in the 50 and 99-level simulations than it has in the 20-level simulation). Simulations have been conducted for 20, 50 and 99 vertical levels, for WRFW-DL and NODIV-VL parameters, representing a total of six simulations. Results have been displayed in supplements, on Figure S5. It can be seen on Figure S5 (left) that all plumes have the same initial volume regardless of vertical resolution, which was not the case in the previous case (c.f. Figure 8a). With a larger vertical extension of the plume at injection, volumes are higher than in the "unique cell injection" cases, but resolution and transport scheme influence in the same way the evolution of plume (considering its volume). Figure S5 (right) shows evolutions of SO_2 highest column vertical profile, similar to Figure 7. This new set of experiments show that, even when getting rid of the initial distorsion due to sharper injection profiles in the simulations with the most refined vertical distributions, the increase in plume volume is much slower in the 99-level simulations than in the 20-level simulations. The final volume is about 4 times smaller in the 99-level simulations compared to their 20-level counterparts. A similar factor in volume reduction is obtained by changing strategy from VL-NODIV to DL-REALW. In total, final plume volume in the worst-case NODIV-VL-20 simulation is about 20 times bigger than final plume volume in the best-case WRFW-DL-99 simulation. Figure S5 (right panel) shows that simulation WRFW-DL-99 is able to reproduce plume thinning under the effect of wind shear, with the plume getting thinner at the end the simulation than it was at the beginning.

4 Conclusion

The Etna eruption of March 18, 2012 has been modelled using the CHIMERE ~~CTM~~ chemistry-transport model in the aim to propose and test strategies to improve representation of atmospheric vertical diffusion which has previously been described in multiple studies (Colette et al., 2011; Boichu et al., 2015; Mailler et al., 2017, e.g.) as over-diffusing, inducing an excessive spread of the simulated plumes. First, the sensitivity to plume injection height and profile have been evaluated, following the plume trajectory with satellites retrievals. It appeared in these tests that the trajectory is highly sensitive to the injection altitude. The intermediate option (injection at 12 km) has been retained and tests and comparisons have been made with this injection

altitude. No significant impact of plume injection profile has been observed and the most simple case of a unique altitude emission has been retained.

In order to reduce the excessive spread of the plume in the vertical direction due to numerical diffusion, three possible approaches have been tested: increasing the number of levels (20, 50 and 99 level simulations have been performed), using the anti-diffusive scheme of Després and Lagoutière (1999) instead of the classical Van Leer (1977) second-order slope-limited scheme, and using realistic vertical winds instead of vertically reconstructed vertical winds, as it is usually done in CTMs (Emery et al., 2011), to the expense of tracer mass conservation. Our results show that, as expected and as already shown in earlier studies, 20 vertical levels are clearly not sufficient to usefully represent any property of vertical transport and dispersion of this plume, and that increasing the number of vertical layers to 50 or to 99 brings significant added value in all respects: horizontal trajectories are improved compared to satellite measurements, vertical diffusion is reduced and maximal concentrations are preserved better. Also very effective is the use of the Després and Lagoutière (1999) anti-diffusive transport scheme instead of the Van Leer (1977) scheme. To our knowledge, this scheme has never been used in chemistry-transport studies, and we show here that this strategy has a very strong potential in preventing simulations to be affected by excessive vertical diffusion without dramatically increasing the number of vertical levels. In our simulations, using the Després and Lagoutière (1999) scheme with 50 levels only has lead to performances that are comparable to the ones obtained with the Van Leer (1977) scheme and 99 levels (compare ~~Fig.~~Figure 7c to ~~Fig.~~Figure 7h or ~~Fig.~~Figure 7f to ~~Fig.~~Figure 7k). With an equivalent number of vertical levels, maximum concentrations in the plume after slightly more that 48 hours of atmospheric transport are about four times as strong in a simulation with the Després and Lagoutière (1999) scheme than in the same simulation but with the Van Leer (1977) scheme. In addition, ~~in principle,~~ increasing vertical resolution ~~is meaningful only in cases where~~ might give a false appearance of accuracy to the result when plume injection altitude is not known with a ~~very good accuracy, while reducing vertical diffusion by other ways do not require increased accuracy in the a prioriknowledge of injection height and profile~~good precision. Finally, it has been shown ~~that~~ than using realistic vertical winds instead of reconstructed vertical winds also improve the horizontal trajectories of the plume, when compared to satellite observations, and reduce plume diffusion in terms of minimum volume containing at least half of the plume mass. It needs to be recalled here that this strategy does not guarantee mass tracer conservation. Even though its impact in this respect has been shown to be quite minor in our study, except in the simulations with 20 vertical levels where it generated an initial excess in tracer mass of about 15%, this characteristic needs to be kept in mind~~and accounted for~~, accounted for and monitored by potential users of this strategy.

These different strategies need to be further studied in different cases to determine whether they can be generalized in CTMs in order to reduce vertical diffusion issues for all pollutants and all kinds of problems, if they are useful only for long-distance transport of inert plumes as we simulated here. For example, how does the Després and Lagoutière (1999) perform in preserving smooth gradients, transitions between the PBL and the free troposphere, or gradients in ozone concentrations at the tropopause ? Regarding the use of realistic vertical wind fluxes interpolated from meteorological outputs, does it help reduce excessive ozone transport through the tropopause as identified by Emery et al. (2011) ? Can this method be generalized to the general chemistry-transport modelling of the troposphere in spite of the mass conservation issues that are intrinsic to this method ?

This study is a call to reopen the issue of limiting vertical mass diffusion in eulerian CTMs: complementary to Zhuang et al. (2018) who emphasized on the need for sufficient vertical resolution, which is confirmed by the present study, we propose two new approaches solve this long-standing problem, including anti-diffusive transport schemes and better representation of vertical mass fluxes throughout the troposphere. Our results show that these new approaches on the vertical direction also permit to reduce horizontal diffusion and that this reduction can be achieved not only by increasing vertical resolution, as shown by these authors, but also by using the Després and Lagoutière (1999) transport scheme as an alternative to classical schemes.

~~Authors contributions~~Code and data availability

The source code for the CHIMERE model (Mailler et al., 2017) is available on: https://www.lmd.polytechnique.fr/chimere/. WRF source code is available on: https://github.com/wrf-model/WRF/. OMI Data (Levelt et al., 2006; McCormick et al., 2013) are available on the NASA GIOVANNI platform: https://giovanni.gsfc.nasa.gov/giovanni/. IASI data (Carboni et al., 2012, 2016) are available contacting the authors. SO_2 (Salerno et al., 2018) flux measurement data are available contacting the authors. Simulation outputs are available contacting the authors.

Authors contributions

S.M. designed the experiments and carried them out. H.G., E.C. and P.S. were responsible for the processing of IASI instrument SO_2 retrieval dataset. G.S., T.C. and S.M prepared eruption emission data. S.M. adapted the model code and performed the simulations. M.L carried out the instruments-model and model-model comparisons. M.L. and S.M. prepared the manuscript and all authors contributed to the text, interpretation of the results and reviewed the manuscript.

Acknowledgements. This study has been supported by AID (Agence de l'Innovation de Défense) under grant TROMPET. Simulations have been performed on the Irene supercomputer in the framework of GENCI GEN10274 project. This work has been supported by the Programme National de Télédétection Spatiale (PNTS, http://www.insu.cnrs.fr/pnts), grant n°PNTS-2019-9.

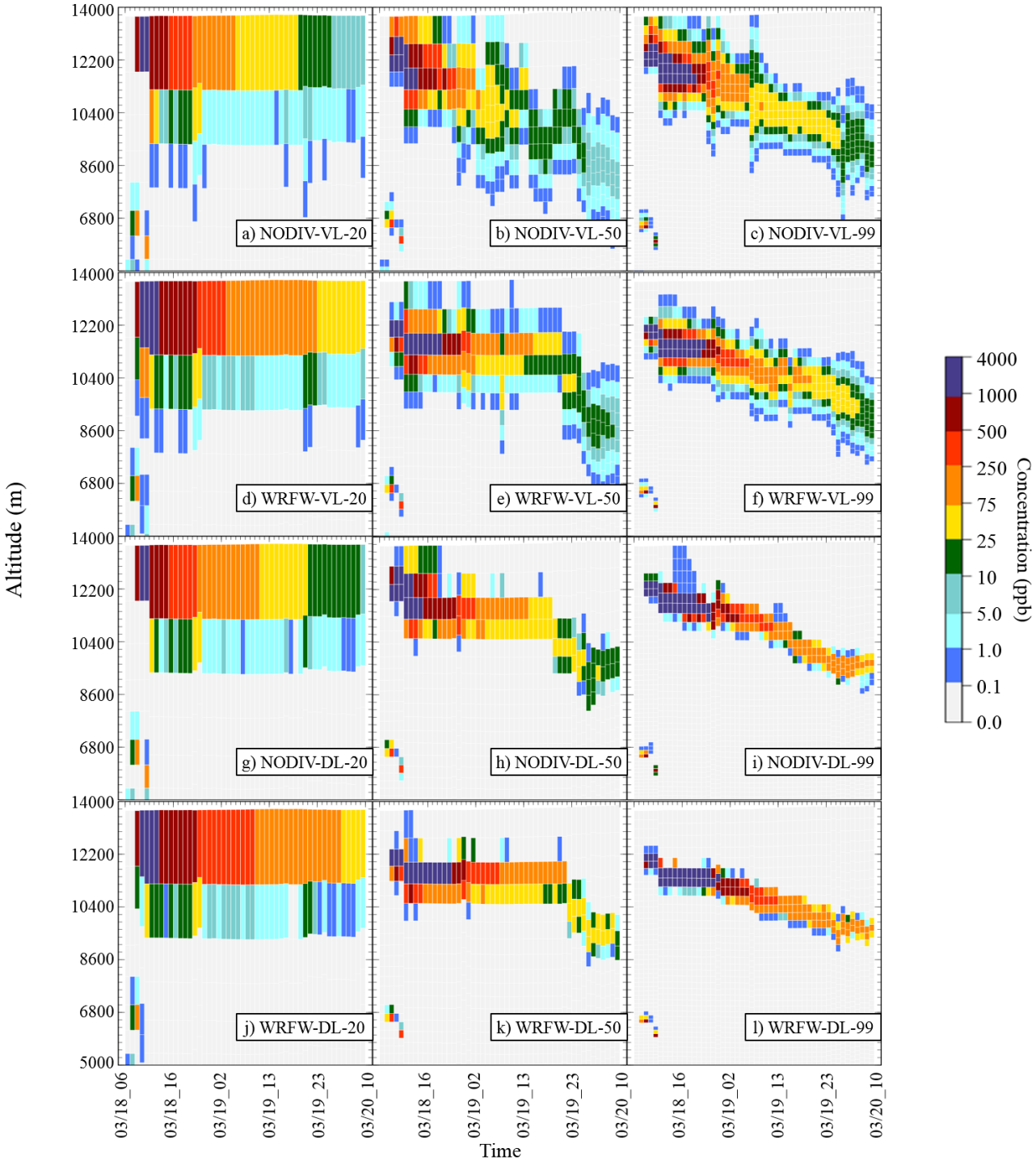

Figure 7. Evolution of SO_2 vertical profile (in ppb) corresponding to the maximum column for each step after the Etna eruption, for each tested model configurations. 1^{st} row: NODIV-VL; 2^{nd} row: NODIV-DL; 3^{rd} row: WRFW-VL; 4^{th} row: WRFW-DL. Left: 20 vertical levels; Center: 50 vertical levels; Right: 99 vertical levels. WRFW simulations values have been corrected to fit NODIV strategy masses.

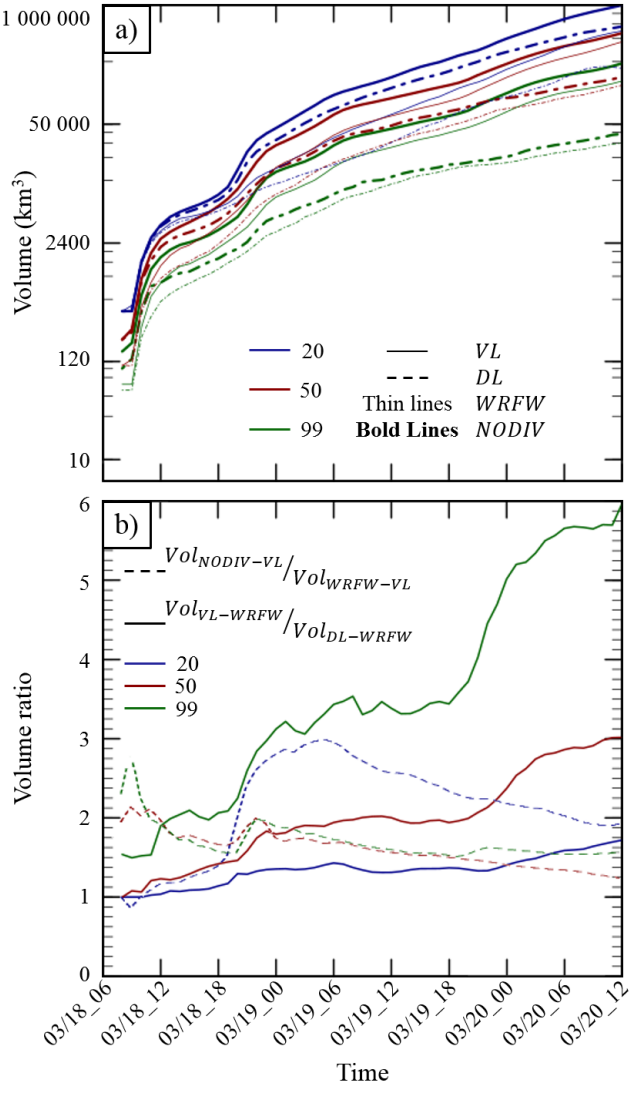

Figure 8. a) Minimum volume evolution calculated for 50 % of SO_2 total mass in the atmosphere. b) Volume ratio evolution by parameters.

References

Boichu, M., Menut, L., Khvorostyanov, D., Clarisse, L., Clerbaux, C., Turquety, S., and Coheur, P.-F.: Inverting for volcanic SO_2 flux at high temporal resolution using spaceborne plume imagery and chemistry-transport modelling: the 2010 Eyjafjallajökull eruption case study, Atmospheric Chemistry and Physics, 13, 8569–8584, https://doi.org/10.5194/acp-13-8569-2013, https://www.atmos-chem-phys.net/13/8569/2013/, 2013.

Boichu, M., Clarisse, L., Péré, J.-C., Herbin, H., Goloub, P., Thieuleux, F., Ducos, F., Clerbaux, C., and Tanré, D.: Temporal variations of flux and altitude of sulfur dioxide emissions during volcanic eruptions: implications for long-range dispersal of volcanic clouds, Atmospheric Chemistry and Physics, 15, 8381–8400, https://doi.org/10.5194/acp-15-8381-2015, https://www.atmos-chem-phys.net/15/8381/2015/, 2015.

Briant, R., Tuccella, P., Deroubaix, A., Khvorostyanov, D., Menut, L., Mailler, S., and Turquety, S.: Aerosol–radiation interaction modelling using online coupling between the WRF 3.7.1 meteorological model and the CHIMERE 2016 chemistry-transport model, through the OASIS3-MCT coupler, Geoscientific Model Development, 10, 927–944, https://doi.org/10.5194/gmd-10-927-2017, https://www.geosci-model-dev.net/10/927/2017/, 2017.

Carboni, E., Grainger, R., Walker, J., Dudhia, A., and Siddans, R.: A new scheme for sulphur dioxide retrieval from IASI measurements: application to the Eyjafjallajökull eruption of April and May 2010, Atmospheric Chemistry and Physics, 12, 11 417–11 434, https://doi.org/10.5194/acp-12-11417-2012, https://www.atmos-chem-phys.net/12/11417/2012/, 2012.

Carboni, E., Grainger, R. G., Mather, T. A., Pyle, D. M., Thomas, G. E., Siddans, R., Smith, A. J. A., Dudhia, A., Koukouli, M. E., and Balis, D.: The vertical distribution of volcanic SO_2 plumes measured by IASI, Atmospheric Chemistry and Physics, 16, 4343–4367, https://doi.org/10.5194/acp-16-4343-2016, https://www.atmos-chem-phys.net/16/4343/2016/, 2016.

Colella, P. and Woodward, P. R.: The piecewise parabolic method (PPM) for gas-dynamical simulations, Journal of Computational Physics, 54, 174–201, 1984.

Colette, A., Favez, O., Meleux, F., Chiappini, L., Haeffelin, M., Morille, Y., Malherbe, L., Papin, A., Bessagnet, B., Menut, L., Leoz, E., and Rouïl, L.: Assessing in near real time the impact of the April 2010 Eyjafjallajokull ash plume on air quality, Atmospheric Environment, 45, 1217 – 1221, https://doi.org/https://doi.org/10.1016/j.atmosenv.2010.09.064, http://www.sciencedirect.com/science/article/pii/S1352231010008502, 2011.

Després, B. and Lagoutière, F.: Un schéma non linéaire anti-dissipatif pour l'équation d'advection linéaire, Comptes Rendus de l'Académie des Sciences - Series I - Mathematics, 328, 939 – 943, https://doi.org/https://doi.org/10.1016/S0764-4442(99)80301-2, http://www.sciencedirect.com/science/article/pii/S0764444299803012, 1999.

Eastham, S. D. and Jacob, D. J.: Limits on the ability of global Eulerian models to resolve intercontinental transport of chemical plumes, Atmospheric Chemistry and Physics, 17, 2543–2553, https://doi.org/10.5194/acp-17-2543-2017, https://www.atmos-chem-phys.net/17/2543/2017/, 2017.

Emery, C., Tai, E., Yarwood, G., and Morris, R.: Investigation into approaches to reduce excessive vertical transport over complex terrain in a regional photochemical grid model, Atmospheric Environment, 45, 7341 – 7351, https://doi.org/https://doi.org/10.1016/j.atmosenv.2011.07.052, http://www.sciencedirect.com/science/article/pii/S1352231011007965, 2011.

Grell, G. A., Peckham, S. E., Schmitz, R., McKeen, S. A., Frost, G., Skamarock, W. C., and Eder, B.: Fully coupled "online" chemistry within the WRF model, Atmospheric Environment, 39, 6957 – 6975, https://doi.org/https://doi.org/10.1016/j.atmosenv.2005.04.027, http://www.sciencedirect.com/science/article/pii/S1352231005003560, 2005.

Guermazi, H., Sellitto, P., Cuesta, J., Eremenko, M., Lachatre, M., Mailler, S., Carboni, E., Salerno, G., Caltabiano, T., Menut, L., Serbaji, M. M., Rekhiss, F., and Legras, B.: Sulphur mass balance and radiative forcing estimation for a moderate volcanic eruption using new sulphate aerosols retrievals based on IASI observations, Atmospheric Measurement Techniques Discussions, 2019, 1–13, https://doi.org/10.5194/amt-2019-341, https://www.atmos-meas-tech-discuss.net/amt-2019-341/, 2019.

Jöckel, P., von Kuhlmann, R., Lawrence, M. G., Steil, B., Brenninkmeijer, C. A. M., Crutzen, P. J., Rasch, P. J., and Eaton, B.: On a fundamental problem in implementing flux-form advection schemes for tracer transport in 3-dimensional general circulation and chemistry transport models, Quarterly Journal of the Royal Meteorological Society, 127, 1035–1052, https://doi.org/10.1002/qj.49712757318, http://dx.doi.org/10.1002/qj.49712757318, 2001.

Klüser, L., Erbertseder, T., and Meyer-Arnek, J.: Observation of volcanic ash from Puyehue–Cordón Caulle with IASI, Atmospheric Measurement Techniques, 6, 35–46, https://doi.org/10.5194/amt-6-35-2013, https://www.atmos-meas-tech.net/6/35/2013/, 2013.

Krotkov, N. A., Li, C., and Leonard, P.: OMI/Aura Sulfur Dioxide SO_2 Total Column L3 1 day Best Pixel in 0.25 degree x 0.25 degree V3, Greenbelt, MD, USA, Goddard Earth Sciences Data and Information Services Center (GES DISC) Accessed: 29/08/2019, https://doi.org/10.5067/Aura/OMI/DATA3008.

Levelt, P. F., van den Oord, G. H. J., Dobber, M. R., Malkki, A., Visser, H., de Vries, J., Stammes, P., Lundell, J. O. V., and Saari, H.: The ozone monitoring instrument, IEEE Transactions on Geoscience and Remote Sensing, 44, 1093–1101, https://doi.org/10.1109/TGRS.2006.872333, 2006.

Mailler, S., Menut, L., Khvorostyanov, D., Valari, M., Couvidat, F., Siour, G., Turquety, S., Briant, R., Tuccella, P., Bessagnet, B., Colette, A., Létinois, L., Markakis, K., and Meleux, F.: CHIMERE-2017: From urban to hemispheric chemistry-transport modeling, Geoscientific Model Development, 10, 2397–2423, https://doi.org/10.5194/gmd-10-2397-2017, 2017.

Mastin, L., Guffanti, M., Servranckx, R., Webley, P., Barsotti, S., Dean, K., Durant, A., Ewert, J., Neri, A., Rose, W., Schneider, D., Siebert, L., Stunder, B., Swanson, G., Tupper, A., Volentik, A., and Waythomas, C.: A multidisciplinary effort to assign realistic source parameters to models of volcanic ash-cloud transport and dispersion during eruptions, Journal of Volcanology and Geothermal Research, 186, 10 – 21, https://doi.org/https://doi.org/10.1016/j.jvolgeores.2009.01.008, http://www.sciencedirect.com/science/article/pii/S0377027309000146, improved Prediction and Tracking of Volcanic Ash Clouds, 2009.

McCormick, B. T., Edmonds, M., Mather, T. A., Campion, R., Hayer, C. S. L., Thomas, H. E., and Carn, S. A.: Volcano monitoring applications of the Ozone Monitoring Instrument, Geological Society, London, Special Publications, 380, 259–291, https://doi.org/10.1144/SP380.11, http://sp.lyellcollection.org/content/380/1/259, 2013.

Menut, L., Bessagnet, B., Khvorostyanov, D., Beekmann, M., Blond, N., Colette, a., Coll, I., Curci, G., Foret, G., Hodzic, a., Mailler, S., Meleux, F., Monge, J.-L., Pison, I., Siour, G., Turquety, S., Valari, M., Vautard, R., and Vivanco, M. G.: CHIMERE 2013: a model for regional atmospheric composition modelling, Geoscientific Model Development, 6, 981–1028, https://doi.org/10.5194/gmd-6-981-2013, http://www.geosci-model-dev.net/6/981/2013/, 2013.

NCEP: NCEP GFS 0.25 Degree Global Forecast Grids Historical Archive, https://doi.org/10.5065/D65D8PWK, 2015.

Pianezze, J., Tulet, P., Foucart, B., Leriche, M., Liuzzo, M., Salerno, G., Colomb, A., Freney, E., and Sellegri, K.: Volcanic Plume Aging During Passive Degassing and Low Eruptive Events of Etna and Stromboli Volcanoes, Journal of Geophysical Research: Atmospheres, 124, https://doi.org/10.1029/2019JD031122, https://agupubs.onlinelibrary.wiley.com/doi/abs/10.1029/2019JD031122, 2019.

Salerno, G., Burton, M., Oppenheimer, C., Caltabiano, T., Randazzo, D., Bruno, N., and Longo, V.: Three-years of SO2 flux measurements of Mt. Etna using an automated UV scanner array: Comparison with conventional traverses and uncertainties in flux retrieval, Journal of Volcanology and Geothermal Research, 183, 76 – 83, https://doi.org/https://doi.org/10.1016/j.jvolgeores.2009.02.013, http://www.sciencedirect.com/science/article/pii/S0377027309000791, 2009.

Salerno, G. G., Burton, M., Di Grazia, G., Caltabiano, T., and Oppenheimer, C.: Coupling Between Magmatic Degassing and Volcanic Tremor in Basaltic Volcanism, Frontiers in Earth Science, 6, 157, https://doi.org/10.3389/feart.2018.00157, https://www.frontiersin.org/article/10.3389/feart.2018.00157, 2018.

Sellitto, P., di Sarra, A., Corradini, S., Boichu, M., Herbin, H., Dubuisson, P., Sèze, G., Meloni, D., Monteleone, F., Merucci, L., Rusalem, J., Salerno, G., Briole, P., and Legras, B.: Synergistic use of Lagrangian dispersion and radiative transfer modelling with satellite and surface remote sensing measurements for the investigation of volcanic plumes: the Mount Etna eruption of 25–27 October 2013, Atmospheric Chemistry and Physics, 16, 6841–6861, https://doi.org/10.5194/acp-16-6841-2016, https://www.atmos-chem-phys.net/16/6841/2016/, 2016.

Sellitto, P., Zanetel, C., di Sarra, A., Salerno, G., Tapparo, A., Meloni, D., Pace, G., Caltabiano, T., Briole, P., and Legras, B.: The impact of Mount Etna sulfur emissions on the atmospheric composition and aerosol properties in the central Mediterranean: A statistical analysis over the period 2000–2013 based on observations and Lagrangian modelling, Atmospheric Environment, 148, 77 – 88, https://doi.org/https://doi.org/10.1016/j.atmosenv.2016.10.032, http://www.sciencedirect.com/science/article/pii/S1352231016308391, 2017.

Skamarock, W. C., Klemp, J. B., Dudhia, J., Gill, D. O., Barker, D. M., Duda, M. G., Huang, X.-Y., Wang, W., and Powers, J. G.: A Description of the Advanced Research WRF Version 3., Tech. rep., NCAR, https://doi.org/doi:10.5065/D68S4MVH, 2008.

Van Leer, B.: Towards the ultimate conservative difference scheme. IV. A new approach to numerical convection, Journal of Computational Physics, 23, 276 – 299, https://doi.org/https://doi.org/10.1016/0021-9991(77)90095-X, http://www.sciencedirect.com/science/article/pii/002199917790095X, 1977.

Zhuang, J., Jacob, D. J., and Eastham, S. D.: The importance of vertical resolution in the free troposphere for modeling intercontinental plumes, Atmospheric Chemistry and Physics, 18, 6039–6055, https://doi.org/10.5194/acp-18-6039-2018, https://www.atmos-chem-phys.net/18/6039/2018/, 2018.